Round Robin Test on tensile and bond behaviour of Steel Reinforced Grout systems

Stefano De Santis[1,*], Francesca Ceroni[2], Gianmarco de Felice[1], Mario Fagone[3], Bahman Ghiassi[4], Arkadiusz Kwiecień[5], Gian Piero Lignola[6], Mattia Morganti[7], Mattia Santandrea[8], Maria Rosa Valluzzi[9], Alberto Viskovic[10]

[1] Roma Tre University, Department of Engineering, Rome, Italy.
[2] University of Naples "Parthenope", Department of Engineering, Napoli, Italy
[3] University of Firenze, Department of Civil, and Environmental Engineering, Firenze, Italy
[4] University of Minho, Department of Civil Engineering, Guimarães, Portugal
Present address: Delft University of Technology, Section Materials and Environment, Delft, The Netherlands
[5] Cracow University of Technology, Department of Civil Engineering, Cracow, Poland
[6] University of Naples "Federico II", Department of Structures of Engineering and Architecture, Napoli, Italy.
[7] CertiMaC c/o ENEA Tecnologie dei Materiali Faenza (TEMAF), Faenza (RA), Italy.
[8] University of Bologna, Department of Civil, Chemical, Environmental and Materials Engineering, Bologna, Italy.
[9] University of Padova, Department of Cultural Heritage, Padova, Italy
[10] University of Chieti-Pescara "G. D'Annunzio", Department of Engineering and Geology, Pescara, Italy.

* Corresponding author. A: Via Vito Volterra 62, 00146 Rome, Italy.
E: stefano.desantis@uniroma3.it. T: +39 06 5733 6387. F: +39 06 5733 3441.

Abstract

Mortar-based reinforcements are an innovative solution for retrofitting existing structures that combine effectiveness, compatibility, and sustainability. Despite the recent spreading of field applications, there is still insufficient knowledge on their fundamental mechanical properties, and a regulatory gap for experimental procedures and design criteria. A Round Robin Test initiative was organized by the Rilem TC 250-CSM (Composites for the Sustainable strengthening of Masonry) to investigate the tensile and bond behaviour of mortar-based composites with basalt, carbon, glass, polyparaphenylene benzobisoxazole (PBO), aramid and steel textiles. This paper presents the tests carried out on Steel Reinforced Grout (SRG) systems, comprising three textile and four mortar types, supplied by three producers. Ten laboratories from Italy, Poland and Portugal were involved for a total of 150 tests, including direct tensile tests on textiles and composites, and single-lap bond tests on masonry substrate. The incidence of the layout of the textile, the mechanical properties of the mortar matrix, the

manufacturing and curing conditions, as well as the testing setup and instrumentation, is discussed to contribute to the optimization of the reinforcement systems and to the development of recommendations for laboratory testing. Finally, results are combined to derive engineering parameters for qualification and design purposes.

Keywords

B. Adhesion; B. Strength; D. Mechanical testing; Fabric Reinforced Cementitious Matrix (FRCM).

1. Introduction

A number of retrofitting solutions are available to repair existing structures, upgrade their strength to comply with increased load demand, safeguard against deterioration and exceptional loads, and improve the resilience to natural hazards, such as earthquakes, subsidence, and floods. Externally bonded reinforcements with composite materials are a particularly effective method, thanks to their high strength-to-weight ratio, relatively fast and easy installation, and versatility (i.e., they are suitable for a broad range of substrate materials and shapes) [1]. Composite reinforcements comprise high strength textiles bonded to the structural members either with a polymeric matrix, giving rise to Fibre Reinforced Polymers (FRPs), or by means of a mortar matrix. Resins allow for relatively easy and fast installation and provide high adhesion to the substrate. Nevertheless, they cannot be applied to wet substrates, have a brittle behaviour, their effectiveness is limited by the glass transition temperature, have no fire resistance, and may deteriorate when exposed to humidity or moisture. On the contrary, mortar-based composites can effectively be installed (with an overall thickness of 10 mm, or even less) on uneven or wet substrates, offer good performance at high temperatures, and are reversible (that is, they can be removed with no or limited damage to the substrate). The first applications to reinforced concrete [2,3], developed to the main purpose of overcoming the drawbacks of epoxy resins, made use of fibre reinforced cement matrices with polymeric additives. The alternative use of lime-based mortars, at the price of lower mechanical performances, provides additional advantages, such as vapour permeability and physical/chemical compatibility with masonry substrates, complying with the preservation criteria required for applications to architectural heritage. On the other hand, inorganic matrices generally provide a weaker adhesion to the

substrate than epoxy resins. In fact, the bond behaviour of mortar based reinforcements is itself more complex than that of FRPs, as failure may occur not only by cohesive debonding within the substrate, but also by slippage of the textile within the matrix, or by detachment at the textile-to-matrix or mortar-to-substrate interface [4,5].

Mortar-based reinforcements are named Textile Reinforced Mortars (TRM) or Fabric Reinforced Cementitious Matrix (FRCM) when comprising carbon [6], glass [7], basalt [8], and PBO [9] fabrics, arranged in the form of open meshes, or Steel Reinforced Grout (SRG) when making use of steel textiles [10]. These latter ones are unidirectional (no bidirectional meshes are available yet) and comprise cords or ropes of Ultra High Tensile Strength Steel (UHTSS). Steel textiles are stiffer and stronger than glass and basalt, and thicker than carbon, aramid and polyparaphenylene benzobisoxazole (PBO), are isotropic (which provides better toughness), exhibit a certain ductility before tensile failure (are less brittle than other fibres), and are more durable in alkaline environment, and need lower cost and energy for production. Nevertheless, they need to be either coated with brass or zinc, or made of stainless steel, to provide protection against salt attack and prevent rusting [11]. Furthermore, since their use in civil engineering for externally bonded reinforcements is more recent than that of carbon and glass, they have not been explicitly included in design codes for epoxy based [12-15] or mortar-based [16] reinforcements yet.

In the last decade, laboratory and field tests have investigated the mechanical properties of Steel Reinforced Grout systems [4,17] and their bond behaviour on concrete [18,19], clay brick [10,20] and masonry [21] substrates. Large scale experiments have proven the effectiveness of SRG for the strengthening of reinforced concrete beams [2,22-24], and masonry arches [25-26] and walls [27-29]. Nevertheless, and despite the already extensive use of SRG in the field [1,30], a better knowledge still needs to be developed on structural performance and durability (which is crucial for the long-term effectiveness of the reinforcement especially when lime-based mortar are used), experimental methods for full characterization, identification of design parameters, qualification and acceptance, and design criteria for structural rehabilitation. As a matter of fact, most of these issues are common to all mortar-based composites, and not limited to the sole SRGs.

For this reason, a Round Robin Test (RRT) initiative was organized by the Rilem Technical Committee 250-CSM (Composites for the Sustainable Strengthening of Masonry) [31] on the tensile and bond

behaviour of mortar-based composites with basalt [32], carbon [33], glass [34], PBO and aramid [35], and steel fabrics. This paper presents the tests carried out on SRG reinforcements by ten laboratories from Italy, Poland and Portugal. In total, 150 tests were carried out, 20 tensile tests on textile specimens, 65 tensile tests on SRG coupons, and 65 single-lap shear bond tests on brick masonry substrate. The systems under investigation comprised three textiles (two stainless steel and one galvanized carbon steel textile, two made of cords and one of ropes) and four matrices (two lime based mortars, one cement mortar and one geopolymer mortar). The work aims at extending the existing database of experimental results thus contributing to the optimization of SRG reinforcements, and to the development of guidelines for testing and design by investigating the following issues:

(i) incidence of the characteristics of the mortar matrix and of the architecture of the textile on the mechanical properties (tensile behaviour) of the composite. The SRG reinforcements that have been tested so far were manufactured with steel cords, while composites with steel ropes have never investigated. Furthermore, no stainless steel textiles have been tested yet;

(ii) bond performance on masonry substrate in terms of strength and failure mode (most of available results deal with the SRG-to-brick bond);

(iii) experimental procedures for fully characterizing the tensile and bond behaviour of mortar-based composites, which are discussed on the base of the large number of tests performed within the RRT and of other available results;

(iv) criteria for identifying engineering parameters for product qualification and structural rehabilitation design.

2. Experimental programme

2.1. Steel textiles and mortar matrices

Three Ultra High Tensile Strength Steel (UHTSS) textiles were used:

- a galvanized (zinc coated) carbon steel textile (G) made of cords, spaced 6.35 mm (Fig. 1a), each of which is obtained by twisting 2 wires around 3 rectilinear ones (Fig. 1d) having 0.108 mm^2 cross section area;

- an AISI 304 stainless steel [36] textile (labelled as S) made of cords, spaced 3.18 mm (Fig. 1b) each of which is obtained by twisting 5 wires having 0.119 mm^2 cross section area (Fig. 1e);
- an AISI 316 stainless steel [37] textile (R) made of ropes (Fig. 1c), obtained by twisting several small wires (Fig. 1f); ropes have a cross section area of 0.69 mm^2 each and are spaced 5 mm.

For each textile, label used in this paper, cord density (c) and spacing (i), surface mass density (γ) and equivalent (design) thickness (t) are listed in Table 1. The textiles were supplied by three different companies.

Four SRG systems were tested, making use of the following mortar matrices:

- a lime based mortar (L), also including geopolymeric binders, such as natural kaolin (hydrated aluminium silicate) and bauxite;
- a geopolymer mortar (G) with natural kaolin and bauxite binders;
- a lime and pozzolan based mortar (labelled as P);
- a fibre-reinforced cement mortar (C) with polymeric additives.

Lime based mortars (P and L) are mainly used for applications to historic substrates, needing relatively low Young's modulus to meet mechanical compatibility requirements, and a high vapour permeability coefficient to fulfil preservation criteria. On the contrary, geopolymer and cement mortars (G and C) may be suitable for applications to modern masonry structures and infill panels, in which higher loads are expected to be transferred to the reinforcement and the vapour permeability is not an issue. The average mechanical properties (and the corresponding Coefficients of Variation, CV) of the matrices are collected in Table 2, which lists the label, the compressive strength (f_{cm}) and the Young's modulus (E_{cm}) from tests on cubic specimens, and the tensile strength (f_{tm}) from three-point bending tests [38] (carried out in Roma Tre University on L, G and P mortars, and at the University of Sannio for C mortar), or provided by technical data sheets.

The SRG systems were constituted by a textile and a mortar provided by the same supplier and named by coupling the corresponding labels. The textile with galvanized steel cords was embedded in the lime based mortar with mineral binders (GL system), and in the geopolymer mortar (GG), the textile with stainless steel cords was embedded in the pozzolan lime mortar (SP), and, finally, the stainless steel rope textile was embedded in the fibre-reinforced cement mortar (RC). The study contributed to the current

knowledge on their mechanical behaviour and on the incidence of textile architecture (cord/rope layout and spacing) and matrix properties (strength and stiffness) on the overall behaviour of SRG composites..

2.2. Overview of experimental study

Ten laboratories, nine of which belonging to public universities and one to a private no-profit research centre (CertiMaC), from Italy, Poland and Portugal were involved in the Round Robin Test programme. Table 3 lists the acronym used for each institution and the tests carried out, according to the following notation: M for mortar matrix characterization, F and T for direct tensile tests on dry textile specimens and SRG composites, respectively, and B for bond tests. Finally, the total number of tests is indicated for each SRG system. For tensile tests on composites and bond tests, superscript S indicates that the specimens were manufactured by the supplier and delivered to the laboratory, while superscript L indicates that the supplier delivered the materials (mortar matrix and steel textile) to the laboratory, which took care of manufacturing the specimens (including the masonry prisms used as substrates for shear bond tests). Specimens of NAP and SAN were manufactured in the same days by the same workers at the laboratory of NAP. The same system was tested by more than one institution (more specifically, four laboratories tested GL and GG systems, two tested SP system, and three RC system) in order to investigate the incidence of different testing setups on test outcomes, and contribute developing standardized testing methodologies for product qualification and material acceptance purposes.

3. Tensile behaviour of steel textiles and SRG composites

3.1. Tests on textile specimens

Direct tensile tests were carried out on S and G textiles by RM3 (Figs. 2a,b) and on R textile by CHI (Fig. 2c) and NAP (Fig. 2d). Five tests were carried out for each series. Aluminium tabs (90 mm × 55 mm × 3 mm) were glued by means of a strong structural adhesive on the ends of the specimens (clamped in the wedges of the testing machine, applying a strong lateral pressure) to ensure uniform stress distribution and prevent sliding in the gripping areas. The corners of the tabs were carefully rounded to inhibit the premature rupture of the steel cords/ropes due to local stress concentrations [17]. Load was applied under

displacement control at 0.02 mm/s rate and recorded by the load cell integrated in the testing machine. Stresses were evaluated by dividing the recorded load by the cross section area of the textile. This latter was calculated as the design thickness of the textile multiplied by the cord spacing and by the number of cords/ropes, or by simply multiplying the area of one individual cord/rope for their number. Strains were derived through the linear variable differential transformer (LVDT) integrated in the testing machine as the recorded displacement divided by the distance between the clamping wedges (which leads to a global strain measure that includes the gripping areas), and validated by comparison with the strain recorded locally by Digital Image Correlation (NAP, RM3), by an extensometer with 50 mm base length (RM3, Figs. 2a,b), or by two LVDTs with 200 mm base length (CHI, Fig. 2c), placed in the middle of the specimen. In each laboratory, the use of more (at least two) measurement methods (providing either global or local strain data) ensured the reliability of test results and allowed for their comparison. The stress-strain curves of all the textiles (shown in Fig. 3 with dotted lines) display an initial elastic behaviour, up to about 60-80% of the tensile strength, followed by a non-linear phase before the peak. In most cases, failure occurred by the nearly simultaneous rupture of the cords/ropes, indicating that the gripping systems succeeded in distributing the load. As an exception, in the tests performed at CHI the progressive, but non-simultaneous, drops after the peak (Fig, 3d) may be due to a non-uniform load distribution which, in turn, led to slightly lower strength than NAP. The individual ropes broke at the same moment with minimum unravelling, indicating that, thanks to the small twisting angle, their wires are loaded uniformly. On the contrary, the tests on S textile show some load drops (Fig. 3c) associated to the premature rupture of some wires (and not actually the entire cord at one time) before the peak, suggesting that the wires may have not been equally loaded (some appear more straight than others). Table 4 collects mean values and corresponding coefficients of variation (CV, in round brackets) of peak stress (f_s) and corresponding load per unit width (F_s), secant Young's modulus (E_s, evaluated between 10% and 50% of f_s), and strain (ε_s) corresponding to peak stress. The mechanical properties of the three textiles investigated within this Round Robin differ largely. The tensile strength of the carbon steel textile is 3191 N/mm^2 and its Young's modulus is 186.5 kN/mm^2, which are both higher than those of the stainless steel textiles (f_s=2083.9 N/mm^2 and E_s=129.7 kN/mm^2 for S textile, and f_s=1114.4 N/mm^2 and E_s=145.4 kN/mm^2 for R textile). The lower Young's modulus of S and R textiles with respect to G textile could be attributed not only to the use of stainless steel, but also to the different layout of the cords (S) or

of the ropes (R), which may have caused a certain geometric deformability, resulting in a lower overall stiffness. As a general trend, the small CVs suggest that both the well-controlled manufacturing process of the steel textiles and the experimental setups allow for a good repeatability of results.

3.2. Tests on SRG composites

Direct tensile tests were carried out to fully characterize SRG composites. Prismatic specimens were manufactured with aluminium or steel moulds and had 10 mm constant thickness (which is a usual thickness for SRG field applications) and 600 mm length. The width of the mortar matrix was 40 mm for GG and GL series, 50 mm for SP series, and 100 mm for RC series. The specimens of GG and GL series comprised 5 cords, corresponding to a width of the textile of 31.75 mm and to an area of 2.67 mm^2, those of SP series had 13 cords (41.28 mm, 7.76 mm^2), those of RC tested at NAP and SAN included 21 ropes (105 mm, 14.49 mm^2), and, finally, those of RC tested at CHI comprised 19 ropes (95 mm, 13.11 mm^2). The textiles were placed in the middle of the thickness taking care of ensuring their linearity. Each coupon was made individually, that is, they were not cut from a larger plate. Specimens were demoulded after 2-3 days and kept wet until 28 days had passed from manufacturing [39]. Then, they were stored in laboratory conditions for at least 7 days before testing. As indicated in Table 3, specimens of SP and RC series were manufactured by the laboratories, while those of GG and GL by the supplier. Five monotonic displacement controlled tests were carried out on each set. The displacement rate was 0.01 mm/s.
Apart from MIN, where the specimens where gripped on the dry textile out of the matrix (Fig. 4a), in all the other institutions the coupons were gripped on the mortar, that is, the entire composite prism was clamped and the load was transferred to the textile through the matrix. In order to ensure a uniform load distribution and avoid mortar crushing in (or near) the gripping areas, each laboratory developed a method for reinforcing the ends of the specimens, either by gluing metal tabs (CER, FIR Figs. 4b,c) or by wrapping with carbon or glass textile bonded with highly deformable polymer (CUT, Fig. 4d) or epoxy resin (BOL, CHI, NAP, PAD, RM3, SAN, Figs. 4e-j). Six laboratories (BOL, CHI, FIR, NAP, RM3, SAN, Figs. 4a,c,e,f,g,i,j) gripped the specimens in the wedges of the testing machine, which apply a lateral pressure by hydraulic or pneumatic clamping, while three (CER, CUT, PAD, Figs. 4b,d,h) placed the specimens between two bolted steel plates, tightened to apply the lateral pressure. The former setup ensured rapid test preparation and high gripping pressure, while the latter was developed to guarantee the

alignment of the tensile load with the axis of the specimen by means of two spherical joints (one at the top and one at the bottom).

The load was measured by the load cell integrated in the testing machine and divided by the cross section area of the textile to calculate the stress. Such a conventional method to define stresses prevents the results from being affected by the variations of the mortar thickness, which are hardly controllable, especially in field applications. Displacements were recorded by the transducer of the testing machine, that provided a global measure from end plate to end plate including the gripping areas, and by potentiometers (Fig 4i), LVDTs (Fig. 4d) or extensometers (Fig. 4e) placed on the mortar matrix, with a measurement base ranging from 50 mm to 250 mm (varying from laboratory to laboratory) excluding the gripping areas. Average strains were then evaluated as the recorded displacement divided by the base length of the devices.

The stress-strain tensile behaviour of the SRG systems, plotted in Fig. 3, is characterized by three response stages: (I) un-cracked, in which the mortar matrix contributes to both load bearing capacity and stiffness; (II) crack development, during which crack pattern develops progressively; and (III) cracked, in which the crack pattern has completely developed. The same behaviour can be observed in different types of mortar-based composites. The relevance of these three stages on the whole tensile behaviour depends on a number of factors, including the tensile strength and the Young's modulus of the matrix, the layout of the fabric, and the cord/fibre-to-mortar bond properties [4,17,40]. As for the SRG systems under study, the first two stages are clearly identifiable in composites comprising stronger mortars, leading to both higher values of σ_I (stress at the transition between stages I and II, i.e., the average value of σ_I is 29% of the average maximum tensile stress for RC, 17% for GC, 14% for GL, and 7% for SP, see Tables 5-8) and larger drops of the stress associated to crack occurrence (systems GG and RC, Figs. 3b,d). Differently, the lower is the strength of the mortar, the lower is its contribution to the response in the un-cracked and crack development stages (system GL, Fig. 3a), to such an extent that it is quite hardly identifiable (system SP, Fig. 3c), which may be due to a relatively lower cord-to-matrix interlocking, and/or to the relatively lower mechanical properties of the mortar.

The results of direct tensile tests on SRG composites are the stress and the strain of the transition points between stages I and II (σ_I, ε_I) and between stages II and III (σ_{II}, ε_{II}), the peak stress (f_t) and the corresponding load per unit width (F_t) and strain (ε_t), the Young's modules in the three stages (E_I, E_{II},

E_{III}), the saturation crack spacing (d) and, finally, the failure mode (FM). Three failure modes were identified, such as rupture near the gripping area (A), rupture in the middle of the coupon (B), and sliding of the textile in the gripping area without tensile rupture (C) (Fig. 5). The transition point between stages I and II corresponds to the development of the first crack, identifiable in the response curve by the first stress drop, while that between stages II and III is at the beginning of the last branch of the response curve. After this point no load drops occur, as no new cracks develop but additional overall strain only induces crack widening. As for the evaluation of the tensile modules of elasticity, E_I and E_{III} are easily calculable as the slope of the first and last portions of the response curve, respectively, while E_{II} is computed through a linear regression of the irregular part of the curve corresponding to stage II. The saturation crack spacing, defined as the mean distance between cracks in the last stage, provides information on the textile-to-matrix load transfer capacity and affects both the structural performance under shear loads (including the reinforcement-to-substrate bond strength) and the durability of the system, as crack development exposes the textile to the aggression of the external environment.

Though the parameters of stages I and II may apparently have limited importance for the rehabilitation design, they indeed provide information on the textile-to-matrix stress transfer capacity and on the contribution of the mortar to the mechanical behaviour of the composite. On the other hand, those related to the last stage and to the peak are related to the maximum attainable load, whose actual exploitation in externally bonded reinforcements, however, relies on the SRG-to-substrate bond strength.

Tables 5-8 report the results of individual tests, the mean values and the CVs calculated both for each set (group of tests carried out in one institution, and nominally identical for both specimen geometry and experimental setup), as well as for all the tests of the same system. At the end of each table, the total average, the total CV and the mean CV are also listed. The total average is the mean of all the experimental data obtained by the different laboratories taken all together, and the total CV is the corresponding coefficient of variation. The mean CV is the average of the coefficients of variation referred to the individual sets of tests performed in the laboratories taken separately. Specimens are labelled according to the notation XY-LLL-N, X and Y being the letters that identify the textile and the matrix, respectively, and LLL the acronym of the institution (Table 3); finally, N is the progressive number of each specimen.

The stress (σ_I and σ_{II}) and, even more, the strain (ε_I and ε_{II}) values of the transition points are associated to high coefficients of variation. On the one hand, this depends on the intrinsic variability of cracking phenomena. On the other hand, the differences among data provided by different laboratories indicate that these results are affected by testing setup and measurement methods, manufacturing and curing conditions, and possible presence of micro-cracks before the beginning of the test, either due to shrinkage or occurring while clamping. Differently, similar crack patterns were observed by all laboratories and on all the tested SRG composites, indicating that the saturation crack spacing can be assessed in a more robust way. Several transversal cracks developed on the whole length and on both sides of the specimens, even if not always regularly spaced. The saturation crack spacing was, on average, 23-27 mm in GG and GL systems (Fig. 6c,d), 31-32 mm in SP system (Fig. 6a), with relatively small differences among laboratories, and 70 mm in RC system (with a larger scatter), which is likely to depend on a weaker rope-to-matrix bond/interlocking (Fig. 6b).

As a general trend, the tensile strength of SRG composites, corresponded to (or are only slightly lower than) those of dry textiles for GL (−11%), GG (−6%) and RC (identical) systems. Differently, for SP systems the maximum stress increased by 18%, suggesting that, in this case, the matrix may have somehow improved the load distribution among the wires within the cords. Indeed, such gain in maximum attained stress should be attributed to the underestimate of the actual tensile strength of the textile derived by tensile tests on dry textile specimens, which, in its turn, may be caused by the nonhomogeneous load distribution amongst the wires of the cords. Clearly, due to the small number of tests performed up to failure, more investigations would be needed to confirm this observation. The values of the modulus of elasticity in the last stage were also similar to those of the Young's modulus of the textile with galvanized cords (−7% for GL, −2% for GG), while slightly larger differences were found for the stainless steel textiles (+38% for SP and −36% for RC). Finally, the stiffening effect of the matrix in the first stages produced a reduction of the peak strain in GL (−19%), GG (−28%) and SP (−23%) systems but not in RC (+15%).

Failure by rupture of the textile either in the middle of the specimen (failure mode B, Fig. 6e) or near the gripping areas (failure mode A, Fig. 6f) occurred when specimens were effectively gripped in the wedges of the testing machine (ensuring a sufficient lateral pressure), and allowed for the full characterization with a reliable assessment of the peak values, which resulted comparable to those of the dry textiles. The

development of cracks while clamping was prevented by proper wrapping or application of metal plates that redistributed the stress, allowing for the detection of the first (uncracked) stage. Clearly, to this purpose, careful manufacturing and curing of the specimens are also needed to ensure that the specimens are straight and shrinkage induced cracking is prevented. The (frequent) failure near the gripping areas (mode A) was not prevented by these end reinforcements but did not strongly compromise the reliability of test results, since similar peak value were found for failure modes A and B. These cracks did not even prevent the correct detection of strain and stiffness values, since several cracks generally developed all along the specimen and were close enough to each other that a large number of them was within the base length of the displacement/strain measurement instruments. On the contrary, premature failure by crushing of the mortar in the gripping areas occurred as a result of ineffective reinforcement (e.g., lack of complete wrapping, Fig. 6g), while slipping of the textile in the mortar matrix (failure mode C) took place due to insufficient lateral pressure (Fig. 6h). This resulted in a significant underestimate of the peak stress and strain values which, therefore, were excluded from statistics. Data of stages I and II were instead considered reliable, because they were derived from LVDTs or extensometers placed on the specimen, excluding the gripping areas. Finally, it is worth to note that no significant difference in the values of CV was observed between the specimens manufactured by the laboratories and those manufactured by the suppliers.

4. SRG-to-brickwork bond behaviour

4.1. Testing setups

Shear bond tests were carried out on SRG systems bonded to masonry prisms made out of five 250 mm × 120 mm × 55 mm clay bricks (having 14.8 N/mm^2 compressive strength, 2.5 N/mm^2 tensile strength and 5.76 kN/mm^2 Young's modulus [40]) and four mortar joints. The laboratories involved in the RRT used different lime mortars for the joints, with compressive strength of about 5 N/mm^2. The reinforcement was bonded for a length (L_b) of 260 mm, leaving an unbonded length of 30 mm from the extremity of the substrate prism on the side of load application, in order to minimize edge effects [31]. The width of the bonded area changed from 40 mm to 100 mm depending on the layout of the textile and the testing setup, and was equal to that of the coupons used in direct tensile tests, that is, the strips of textile comprised 5

cords for GL and GG, 13 cords for SP, and 19 or 21 ropes for RC systems (the values of the cross section areas, therefore, coincide to those specified in Section 3.2.). The reinforcement was applied to one side of the brickwork prism following a standard wet lay-up procedure, according to the recommendations provided by the suppliers. Before installation, the substrate was cleaned with a metallic brush, dust was removed with compressed air, and the surface was wet with water, without any other specific surface treatments (application of primers, sandblasting, bush-hammering, etc.). A first 5 mm thick layer of mortar matrix was applied by means of aluminium or wooden frameworks. The textile was then placed by hand and pressed slightly into the fresh mortar, to allow its protrusion through the voids between cords/ropes. The alignment of cords/ropes was ensured. Finally, a 5 mm thick layer of mortar was applied on top. Specimens were kept wet for 28 days and then stocked for at least 7 days in the laboratory before testing. As for the coupons subjected to tensile tests, specimens of SP and RC series were manufactured by the laboratories, while those of GG and GL series by the supplier.

Tests were carried out with a single lap scheme, by blocking the specimen and pulling the unbonded textile from below (CER, CHI, CUT, RM3, Figs. 7a-d) or above (BOL, NAP, MIN, FIR, PAD, Figs. 7e-i) using a universal testing machine, with the only exception of SAN that used a horizontal setup provided with a manual movable actuator (Fig. 7j). Depending on available facilities, laboratories designed stiffened steel frames that ensured the alignment between the tensile load applied to the unbonded textile and the middle plane of the reinforcement. By doing so, the reinforcement-to-substrate interface was subjected to a pure shear stress, such that a pure shear stress was applied at the SRG-to-substrate interface. For this purpose of avoiding rotations during test execution, the masonry prism was blocked by steel plates either at the back and at the front (CER, CUT, RM3, SAN, Figs. 7a,c,d,j), or at the top and at the bottom (BOL, FIR, MIN, NAP, PAD, Figs. 7e,f,g,h,i), the latter setup inducing a pre-compression in the substrate, in addition to the compression that arises during test execution in any push-pull testing scheme. The unbonded textile was left dry, that is, it was not impregnated with epoxy resin or mortar. Its end was reinforced with metal plates for clamping or with GFRP (NAP), to ensure that a uniform load was transferred to all the cords/ropes and avoid their premature rupture in the gripping area.

As for direct tensile tests, the load was recorded by the load cell integrated in the testing machine and divided by the cross section area of the textile to calculate the stress. The relative displacement (slip) between the textile and the substrate at the loaded end of the reinforcement was recorded by LVDTs

(BOL, CHI, CUT, FIR, MIN, NAP, RM3) or potentiometers (PAD). One end of the device was fixed to the substrate and the other one to the textile (making use of metal plates), out of the bonded area, at a certain distance (ℓ) from the first bonded section, varying from laboratory to laboratory depending on the experimental setup. The slip was then calculated as the recorded displacement minus the elastic elongation of the unbonded textile $\varepsilon \times \ell$, ε being evaluated as the applied load divided by the section area and the Young's modulus E_s of the textile derived from tests on dry textile specimens (i.e., assuming that all the cords were equally loaded). Differently, in SAN four resistive strain gauges were glued to the textile along the bonded area (at 20, 80, 140, 200 mm from the first bonded section) and the reinforcement-to-substrate slip was calculated by integrating the strains, that is, adding up the strains multiplied by the spacing between gauges.

In CUT, NAP, RM3 and SAN Digital Image Correlation (DIC) was also used to record the displacement field on the surface of the specimen and validate the slip data provided by traditional devices. The possibility of applying DIC, as well as other unconventional measurement techniques, to the mechanical characterization of composites is still at a relatively early stage [42-46] and is out of the scope of the present paper.

4.2. Results

The results of shear bond tests are the stress at failure (or bond strength, f_b), the corresponding load per unit width (F_b) and slip (s), and the exploitation ratios of the tensile strength (η_s and η_t), referred to dry textiles ($\eta_s=f_b/f_s$) or to SRG composites ($\eta_t=f_b/f_t$). These data are listed in Tables 9-12 together with the failure mode, indicated for each test according to the following classification: debonding with cohesive failure of the substrate (A), debonding at the matrix-to-substrate (B) or at the textile-to-matrix (C) interface, textile slippage within the matrix without (D) or with (E) cracking of the outer layer of mortar (very similar to each other and sometimes barely distinguishable, both being basically governed by the sliding of the cords/ropes), and, finally, tensile rupture of the textile out of the bonded area (F) (Fig. 8). As for tensile tests, results are reported for each individual test, together with the mean values and the corresponding CV for each series of tests carried out in a single institution. Finally, the overall mean, the mean of the CVs of each set and the CV of all the individual tests are calculated. In the tables, the

specimens are labelled according to the notation XY-B-LLL-N, which corresponds to that used for direct tensile tests with the addition of letter B (standing for the brickwork substrate).

The SRG reinforcement with galvanized steel textile and lime based mortar (GL) displayed an average bond strength of 2628.3 N/mm^2, corresponding to exploitation ratios of η_s=84% and η_t=94% and to a load per unit width of 219.7 kN/m (Table 9). The stress-slip response curves display a good agreement (Fig. 9a) with the exception of three of them that are lower than the others from the beginning, associated to tests in which premature localized debonding occurred either at the mortar-to-substrate or at the textile-to-mortar interface, or in which the outer layer of mortar cracked prematurely. Nevertheless, the bonded length after cracking was long enough that the failure load was not significantly affected by this early occurrence of local damage. Conversely, the response appears much more scattered beyond 1mm slip and 1800 N/mm^2 stress, at the activation of the debonding process. Different failure modes also took place. The tensile rupture of the textile occurred in RM3 (Fig. 10f), and in BOL this was associated to the detachment between textile and matrix and expulsion of the outer mortar layer. Sliding and cracking of the mortar were observed at MIN, while debonding at the matrix-to-textile interface was reported by PAD (Fig. 10b). Consistently, the loads attained in BOL and RM3 were higher than those recorded at MIN and PAD, the exploitation ratios being 91-95% in the former case (BOL, RM3) and 72-75% in the latter one (MIN, PAD). Even if a combination of failure modes was often observed (Table 9), the variation of results amongst laboratories was acceptable since the global CV was 15.4%. Furthermore, a very low scatter amongst the specimens tested in the same institution was observed in the tests of BOL, PAD, and RM3 (i.e., CV=1-5%).

The mean stress at debonding of GG system (galvanized steel textile and geopolymer mortar) was about 5% lower than the strength of GL system (Table 10), corresponding to η_s=78%, η_t=83%. The initial stiff bond behaviour (Fig. 9b) was followed by clearly identifiable stress drops at the occurrence of cracks in the matrix (CUT, Fig. 10c, FIR, Fig. 10e) or in the substrate (RM3, Fig. 10a). Differently from the previous case (GL), variations from laboratory to laboratory in terms of response curves were relatively small and also the bond strength had a low scatter (global CV=14.3%), even if different failure modes were observed also in this case (Table 10).

SP and RC systems exhibited significantly lower bond strength than the galvanized steel cords, i.e. −62% for SP and −64% for RC systems with respect to GL. The stress-slip curve of SP system, comprising

stainless steel cords and lime and pozzolan mortar matrix (Fig. 9c) was characterized by an initial stiff phase up to a slip of about 1.5 mm. Then, the textile slipped out of the matrix (Fig. 10d) with a slight increase of the stress (the curves are basically horizontal), which is associated to the cord-to-mortar friction. The maximum stress was, on average, 951.1 N/mm^2, corresponding to a maximum load per unit width of 178.8 KN/m and exploitation ratios of η_t=46% and η_s=39% (Table 11).

RC reinforcement (stainless steel ropes and cement mortar) displayed a bond strength of 949.3 N/mm^2, corresponding to 85% of its tensile strength and to a load per unit width of F_t=131 kN/m, with relatively low scatter (Table 12). The relatively lower values recorded at CHI are probably related to a non-homogeneous load in the textile, as revealed by the consecutive load drops associated to the rupture of the cords in the post-peak phase (Fig. 9d). Failure occurred by tensile rupture of the textile also at SAN, while in NAP textile slippage took place, associated to a slight stress decrease in the post peak stage. Despite the small scatter of results attained by CHI, NAP and SAN, the tests carried out at SAN gave the highest bond strength and the lowest CV amongst the laboratories testing the RC system, indicating the good stability of the horizontal pull-push setup, which limits the influence of detailing and loading eccentricity. Conversely, large differences were found for the slip values, those recorded at SAN being lower than those of CHI and NAP. On the one hand, this may be due to rotations, deflections or setting of the LVDTs (or of the metal plates where they were fixed), inducing an overestimate of the actual displacement at CHI and NAP. On the other hand, at SAN, the strain gauges may have provided an underestimate of the slip, as they were bonded only to one cord in for points (thus providing local measurements), may have partially detached or may have failed in capturing possible strain concentrations near the loaded end of the bonded area.

The results of the RRT indicate that a combination of factors affect the bond strength and the failure mode of externally bonded SRG reinforcements, including (i) the strength of the textile and the cord-to-mortar bond/interlocking, (ii) the mechanical properties of the mortar matrix, (iii) the roughness of the substrate, and (iv) the experimental setup and the manufacturing and curing conditions.

The sliding of the textile from the matrix observed at NAP on RC system may be attributed to the relatively low cord-to-mortar interlocking provided by the stainless steel ropes, whose surface is smoother than that of the cords. On the other hand, the high strength of the fibre-reinforced polymer modified cement mortar has impeded this slippage at CHI and SAN, where failure occurred by rupture of the textile

whose tensile strength was lower than that of the other textiles under investigation. Similarly, the sliding failure observed on SP system at RM3 indicates a relatively weaker interlocking of the cords with the matrix with lower mechanical properties.

The incidence of the mechanical properties of the matrix is further highlighted by the different bond behaviour displayed by systems GG and GL in the tests carried out at RM3. The specimens of both series comprised the same textile (galvanized steel cords), were manufactured by the supplier (with the same manufacturing and curing conditions for brickwork prisms and reinforcements) and tested by the same laboratory with the same experimental setup. The reinforcement with geopolymer mortar (GG) failed by combined failure mode with cohesive debonding within the substrate (a very thin layer of brick and mortar being peeled off) and detachment at the composite-to-substrate interface (Figure 10a). The mean stress in the textile at failure was 2456.7 N/mm^2 corresponding to exploitation ratios of η_s=77% and η_b=82%. Differently, the GL system (with lime based mortar) failed by tensile rupture of the textile at 3024.9 N/mm^2 bond strength (η_s=94%, η_b=95%). These results suggest that the stiffer matrix may have caused stress concentrations that activated the cohesive debonding process within the substrate. The more deformable mortar, instead, allowed for a uniform distribution of the stress at the reinforcement-to-brickwork interface and to the attainment of a higher bond strength, consistently with the outcomes of previous research studies carried out on Fibre Reinforced Polymers bonded to similar substrates with different polymeric matrices [47]. Furthermore, it should be considered that the geopolymer mortar (G) was mainly developed for applications to concrete substrates, typically characterized by a lower adsorption rate than the masonry. Therefore, a relatively high amount of water might have been lost during curing, which, also due to the small thickness of the matrix layer, may have caused a reduction of its mechanical properties. On the contrary, the lime-based mortar (L), being developed for applications to masonry, is less sensitive to the relatively high water adsorption rate of the masonry substrate.

The bond strength revealed by GL and GG systems in this RRT is 2-3 times higher than that exhibited in previous investigations [10] by these same systems bonded to the same brick substrate used to manufacture the masonry prisms (so, on homogeneous substrate), for a shorter bonded length (200 mm instead of 260 mm). This load increase was probably due both to the higher roughness of the masonry substrate induced by the presence of mortar layers and to the longer bonded length, but further experimental data need to confirm these outcomes.

5. Identification of qualification parameters

Despite the knowledge developed so far on the mechanical behaviour, and the number of applications that have already been realized for the protection of the built heritage, the qualification and acceptance of mortar-based composites is still an open issue since no guidelines are available, except the US standard AC434 [48]. This regulatory gap represents in some countries (e.g., Italy) a formal obstacle to their use with full rights in the design of rehabilitation interventions. A procedure was recently proposed in [49] and it is herein applied to the SRG reinforcements under investigation.

The characteristic (5% fractile) strength, f_k is derived from the results of the shear bond tests as the mean value of the stress at failure (f_b) minus k_n times the corresponding standard deviation, k_n being a fractile coefficient that depends on the number of specimens [50]. The qualification strain, ε_k is the strain corresponding to f_k on the mean curve derived from tensile tests on SRG composites. Finally, the secant stiffness is defined as $E_k=f_k/\varepsilon_k$. In the method, it is assumed that the load is transferred by the structure to the SRG system by shear, such that bond failure may occur. This situation take place in several structural applications, such as the reinforcement of masonry walls under in-plane or out-of-plane loads, arches and vaults, lintels, etc. The confinement and the applications that make use of mechanical end anchors should instead be excluded (i.e., the design parameters cannot be derived through this procedure), since in these cases the bond failure is not an issue and the system is expected to fail by tensile rupture of the steel textile.

The qualification parameters (f_k, ε_k and E_k) for the four SRG systems investigated in this study are listed in Table 13, together with the load per unit width F_k corresponding to the qualification stress. The number of specimens available from bond tests and the corresponding fractile coefficient k_n are also specified. When this latter is not directly provided by Eurocode 0, a linear interpolation was performed between recommended values. The standard deviation was evaluated on the entire set of tests. Clearly, since performing the tests in different laboratories introduces a certain variability by itself, this scatter measure is likely to be larger than that expected from tests carried out in one official laboratory for product qualification or material acceptance purposes.

For all the systems, the qualification point belongs to the third stage of the tensile behaviour, where the envelopes of the response curves (Fig. 11) show a smooth trend and a relatively low scatter. This is due to

the fact that the cracks, whose occurrence results in both the stress drops and increased the variability from test to test, have already developed. Therefore, slight variations of cracking, manufacturing and curing, and experimental setups are expected to provide limited modifications of the qualification parameters. Finally, the secant stiffness E_k is close to the Young's modulus of the last stage E_{III}.

The performances of the four SRG systems considered in this RRT are compared in Fig. 12 in terms of load per unit width and strain, corresponding to tensile strength, and average and characteristic bond strength. The maximum load per unit width ranged between 154 kN/m to 460 kN/m (Figure 12a), and the corresponding strain was between 1.2% and 1.8% (Figure 12b). The qualification load was between 98 kN/m and 160 kN/m, and the strain varied from 0.23% to 0.96%. As said before, the values of the maximum load attained on dry textile specimens agree with (or are only slightly lower than) those reached on SRG composites, with the only exception of SP system, in which the presence of the mortar matrix allows for an increase of the tensile strength.

Furthermore, it is worth noting that the maximum load per unit width given by the tensile tests was found for the SP system, despite the maximum tensile stress reached in the bond tests was lower than that of GL and GG composites, thanks to the higher thickness (i.e., to the lower spacing between cords). On the other hand, this system has the lower qualification load and strain, due to the occurrence of sliding failure. SRG systems made of galvanized steel cords attained the highest exploitation ratios ($\eta_t = f_b/f_t$, i.e. the ratio of to the mean debonding stress to the means tensile tests of the composite system): 94% in case of lime based mortar (GL) and 83% in case of geopolymer mortar (GG). Comparable efficiency was attained by the stainless steel ropes embedded in the cement mortar (RC system, η_t=85%), while the stainless steel cords embedded in the lime and pozzolan mortar (SP system) attained an η_t of 41% (Figure 12c). The efficiency referred to the qualification stress is also plotted in Figure 12c and it was 62-67% for GL, GG and RC systems and 23% for SP system.

6. Conclusions

The tensile and bond behaviour of four Steel Reinforced Grout (SRG) composites was investigated in a Round Robin Test programme involving ten laboratories. The study provided information on the role played by the layout of the textile, the properties of the mortar matrix, and the testing setup and

instrumentation. The mechanical parameters of SRG composites vary widely depending on the characteristics of their components (strength, Young's modulus, textile layout, etc.). The results achieved in this study reflect the broad variability of the systems available in the market and the importance of performing the accurate characterization of each of them before use.

Direct tensile tests indicated that:

- the tensile behaviour is characterized by three response stages: (I) un-cracked; (II) crack development, and (III) cracked;
- the better is the cord-to-mortar interlocking and the higher is the tensile strength of the matrix, the larger is its contribution to the strength and stiffness of the system in stages I and II;
- the peak value and the stiffness in the last stage basically agree with those of the dry textiles, a larger mismatch only arising when a certain inhomogeneity of the load amongst the wires may lead to underestimate its strength when tested alone (not embedded in the mortar matrix). In this case, higher stress values are attained by the coupon thanks to the stress redistribution provided by the mortar.
- The clamping method is crucial to achieve a full mechanical characterization of SRG composites by means of tensile tests. In order to reliably assess the peak values, specimens need to be gripped on the mortar (that is, all the coupon has to be clamped) with enough lateral pressure that prevents the textile from sliding. To detect the first (uncracked) stage, adequate wrapping with FRP is also necessary that avoids mortar crushing in the gripping areas. Due to the high pressure in the gripping areas, cracks may develop at the ends of the specimens during the test, despite the FRP reinforcement, but this does not significantly affect the maximum attainable stress.
- Strain, stiffness, and crack spacing can be accurately measured by displacement/strain transducers placed on the mortar matrix, since numerous cracks develop, close enough to each other that a large number of them is within the base length of the instruments.

Single-lap shear bond tests carried out on brickwork substrate indicated that:

- the structural performance of the reinforcements (in terms of maximum load per unit width) ranged between 130.6 kN/m and 226.4 kN/m;
- the efficiency of the systems was expressed by the exploitation ratios η_s and η_t, referring to the tensile strength of the textile and of the composite, respectively, ranging between 84% and 94%

when bond failure occurred by detachment and the reinforcement-to-substrate or at the textile-to-matrix interface. A lower efficiency (41%) was instead associated to the occurrence of textile sliding.

- The bond behaviour (strength and failure mode) depends on the strength of the textile and the cord-to-mortar bond/interlocking, the mechanical properties of the matrix, the manufacturing and curing conditions, including the proper preparation of the substrate before installation, and the experimental setup. More specifically: (i) a relatively low cord-to-mortar interlocking (caused by a smooth surface of the cord or by a low strength of the matrix) may provide sliding of the textile from the matrix; (ii) the presence of mortar joints leads to the attainment of a higher bond strength with respect to homogeneous brick substrate.
- Apart from the physiological variability of experimental results, the occurrence of different failure modes for the same reinforcement system should be attributed to the variations of manufacturing and curing conditions and to the differences in the experimental setups. The former may affect the strength of the mortar and the bond strength between the matrix and the substrate. The latter may be responsible of a parasitic normal stress at the reinforcement-to-substrate interface and the non-uniform load among the steel cords/ropes.
- The correct alignment ensures the reliability of the slip measured by displacement transducers, provided that these are firmly fixed to both the textile and the substrate. Unconventional strain/displacement measurement methods, such as Digital Image Correlation (DIC), are emerging as promising techniques to be integrated with traditional devices.
- Further research is still needed to identify an effective transfer length, if exists. Field tests would also help understand the actual bond behaviour in full-scale applications and under the less controllable conditions (variability of the substrate, humidity during installation and curing of the mortars) of the construction site.

For the four SRG systems tested in this study, the qualification points belong to the third stage of the tensile response, the stress value roughly being in the 60-70% range of the tensile strength, except of one case that failed by sliding of the cords within the matrix with lower exploitation (22%). Since, at this stage, the crack pattern has fully developed, the trend of the curve is smooth and there is limited scatter from test to test. Therefore, slight variations of crack occurrence, manufacturing and curing, and

experimental setups are expected to provide limited modifications of the qualification parameters (stress, strain, and secant stiffness).

The role played by the properties of the textile and of the mortar matrix on the bond behaviour (strength, failure mode) indicates that every SRG system needs to be characterized and qualified individually in order to derive reliable design parameters. On the other hand, analytical relationships should be developed to estimate the bond strength for the design of rehabilitation interventions. Since failure may occur not only in the substrate but also within the thickness of the reinforcement system, the theoretical approach developed for FRPs cannot be directly extended to mortar-based composites, but should be extended by introducing the dependency from the mechanical properties of the matrix (tensile and compressive strength) and the layout of the textile (spacing, roughness).

Despite these open issues, the knowledge developed so far demonstrates the effectiveness of SRGs for the reinforcement of existing structures, their capability of overcoming the drawbacks of epoxy resin based composites, the potentiality of being integrated in the ordinary maintenance works of the façades (as they can be included in the thickness of the plaster layer), and the possibility of complying with the principles of conservation for applications to architectural heritage.

Acknowledgements

The cooperation of the industrial partners G&P Intech S.r.l., Kerakoll S.p.A. and Mapei S.p.A. for providing materials and cofunding and that of SanMarco-Terreal (Italy) for providing the clay bricks for bond tests are kindly acknowledged. The authors would like to thank the researchers from participating institutions that cooperated to the tests: Francesca Roscini (Roma Tre University), Matteo Scafé (ENEA Tecnologie dei Materiali Faenza (TEMAF), Faenza), Mattia Santandrea (University of Bologna), Gina Zuccarino (University of Chieti-Pescara), Giovanna Ranocchiai (University of Firenze), Łukasz Hojdys and Piotr Krajewski (Cracow University of Technology), Roberto Cuzzilla (University of Sannio), Alberto Balsamo and Ivano Iovinella (University of Napoli).

References

[1] Valluzzi MR, Modena C, de Felice G. Current practice and open issues in strengthening historical buildings with composites. Mater Struct 2014;47(12):1971-1985.

[2] Huang X, Birman V, Nanni A, Tunis G. Properties and potential for application of steel reinforced polymer and steel reinforced grout composites. Compos Part B-Eng 2005;36:73-82.

[3] Triantafillou TC, Papanicolaou CG. Shear strengthening of reinforced concrete members with textile reinforced mortar (TRM) jackets. Mater Struct 2006;39(285):93-103.

[4] de Felice G, De Santis S, Garmendia L, Ghiassi B, Larrinaga P, Lourenço PB, Oliveira DV, Paolacci F, Papanicolaou CG. Mortar-based systems for externally bonded strengthening of masonry. Mater Struct 2014;47(12):2021-2037.

[5] Carozzi FG, Poggi C. Mechanical properties and debonding strength of Fabric Reinforced Cementitious Matrix (FRCM) systems for masonry strengthening. Compos Part B-Eng 2015;70:215-230.

[6] D'Ambrisi A, Feo L, Focacci F. Experimental and analytical investigation on bond between Carbon-FRCM materials and masonry. Compos Part B-Eng 2013;46:15-20.

[7] Carozzi FG, Milani G, Poggi C. Experimental investigation of tensile and bond properties of Carbon-FRCM composites for strengthening masonry elements. Compos Struct 2014;107:711-25.

[8] Balsamo A, Di Ludovico M, Prota A, Manfredi G. Masonry walls strengthened with innovative composites. American Concr Inst, ACI SP 2011;2(275):769-86.

[9] D'Antino T, Carloni C, Sneed LH, Pellegrino C. Matrix-fiber bond behavior in PBO FRCM composites: A fracture mechanics approach. Eng Fract Mech 2014;117:94-111.

[10] De Santis S, de Felice G. Steel reinforced grout systems for the strengthening of masonry structures. Compos Struct 2015;134:533-548.

[11] De Santis S, de Felice G, Napoli A, Realfonzo R. Strengthening of structures with Steel Reinforced Polymers: a state-of-the-art review. Compos Part B-Eng 2016;104:87-110.

[12] FIB, Fédération internationale du béton. Fib Bulletin No. 14. Externally bonded FRP reinforcement for RC structures. Lausanne, Switzerland, 2001.

[13] American Concrete Institute. ACI 440.2R-08 Guide for the design and construction of externally bonded FRP systems for strengthening concrete structures. Farmington Hills, MI, USA, 2008.

[14] American Concrete Institute. ACI 440.7R-10 Guide for the design and construction of externally bonded Fibre-Reinforced polymer systems for strengthening unreinforced masonry structures. Farmington Hills, MI, USA, 2010.

[15] CNR, Italian National Research Council. CNR-DT200 R1/2013. Guide for the design and construction of externally bonded FRP systems for strengthening existing structures. Rome, 2013.

[16] American Concrete Institute. 549.4R-13 Guide to design and construction of externally bonded Fabric-Reinforced Cementitious Matrix (FRCM) systems for repair and strengthening concrete and masonry structures. Farmington Hills, MI, USA, 2013.

[17] De Santis S, de Felice G. Tensile behaviour of mortar-based composites for externally bonded reinforcement systems. Compos Part B-Eng 2015;68:401-413.

[18] Matana M, Nanni A, Dharani LR, Silva P, Tunis G. Bond Performance of steel reinforced polymer and steel reinforced grout. In: Proceedings Int. Symposium on Bond Behaviour of FRP in Structures (BBFS), Hong Kong, China, 2005.

[19] Stievanin E, Da Porto F, Panizza M, Garbin E, Modena C. Bond characterization between historical concrete substrate and SRG/SRP strengthening systems. In: Proceedings of 5th Int. Conference on Structural Engineering, Mechanics and Computation SEMC2013, Cape Town, South Africa, 2013.

[20] Razavizadeh A, Ghiassi B, Oliveira DV. Bond behavior of SRG-strengthened masonry units: Testing and numerical modeling. Constr Build Mater 2014;64:387-397.

[21] De Santis S, de Felice G. Bond behaviour of Steel Reinforced Grout strengthening systems applied to the extrados of masonry vaults. In: Proceedings of the 10th International Conference on Structural Analysis of Historical Constructions SAHC 2016, Leuven, Belgium.

[22] Da Porto F, Stievanin E, Garbin E, Valluzzi MR. SRG application for structural strengthening of RC beams. ACI SP 2012;286:119-132.

[23] Balsamo A, Nardone F, Iovinella I, Ceroni F, Pecce M. Flexural strengthening of concrete beams with EB- FRP, SRP and SRCM: Experimental investigation. Compos Part B-Eng, 2013;46:91-101.

[24] Napoli A, Realfonzo R. Reinforced concrete beams strengthened with SRP/SRG systems: Experimental investigation. Constr Build Mater 2015;93:654-677.

[25] Borri A, Casadei P, Castori G, Hammond J. Strengthening of brick masonry arches with externally bonded steel reinforced composites. J Compos Constr 2009;13(6):468-475.

[26] Ramaglia G, Lignola GP, Balsamo A, Prota A, Manfredi G. Seismic strengthening of masonry vaults with abutments using Textile Reinforced Mortar. J Compos Constr 2016;04016079.

[27] Borri A, Castori G, Corradi M. Shear behavior of masonry panels strengthened by high strength steel cords. Constr Build Mater 2011;25(2):494-503.

[28] De Canio G, de Felice G, De Santis S, Giocoli A, Mongelli M, Paolacci F, Roselli I. Passive 3D motion optical data in shaking table tests of a SRG-reinforced masonry wall. Earthq Struct 2016;10(1):53-71.

[29] De Santis S, Casadei P, De Canio G, de Felice G, Malena M, Mongelli M, Roselli I. Seismic performance of masonry walls retrofitted with steel reinforced grout. Earthq Eng Struct D 2016;45(2):229-251.

[30] Agneloni E, Casadei P. Case studies on advanced composite materials for civil engineering and architectural applications. Structural Engineering International: Journal of the International Association for Bridge and Structural Engineering (IABSE) 2011;21(3):271-278.

[31] De Santis S, Carozzi FG, de Felice G, Poggi C. Test methods for Textile Reinforced Mortar systems. Submitted to Compos Part B-Eng.

[32] Lignola GP, Caggegi C, Ceroni F, De Santis S, Krajewski P, Lourenço PB, Morganti M, Papanicolaou CG, Pellegrino C, Prota A, Zuccarino L. Performance assessment of basalt FRCM for retrofit applications on masonry. Submitted to Compos Part B-Eng.

[33] Carozzi FG, Bellini A, D'Antino T, de Felice G, Focacci F, Hojdys L, Laghi L, Lanoye E, Leone M, Panizza M, Poggi C. Experimental investigation on tensile and shear bond properties of Carbon-FRCM composites applied on masonry substrates. Submitted to Compos Part B-Eng.

[34] Leone M, Aiello MA, Balsamo A, Carozzi FG, Ceroni F, Corradi M, Ranocchiai G, Frajewski P, Garbin E, Oliveira DV, Papanicolaou CG, Roscini F, Saenger D, Gattesco N, Gams M. Experimental study of glass fibre reinforced mortar system on masonry substrate. Submitted to Compos Part B-Eng.

[35] Caggegi C, Carozzi FG, De Santis S, Fabbrocino F, Focacci F, Hojdys L, Lanoye E, Zuccarino L. Experimental analysis on tensile and bond properties of PBO and Aramid fabric reinforced cementitious matrix for strengthening masonry structures. Submitted to Compos Part B-Eng.

[36] ASTM International. ASTM A240 / A240M-16a, Standard Specification for Chromium and Chromium-Nickel Stainless Steel Plate, Sheet, and Strip for Pressure Vessels and for General Applications, ASTM International, West Conshohocken, PA, 2016.

[37] ASTM International. ASTM A276 / A276M-16a, Standard Specification for Stainless Steel Bars and Shapes, ASTM International, West Conshohocken, PA, 2016.

[38] CEN, European Committee for Standardization. EN 1015-11:1999. Methods of test for mortar for masonry. Determination of flexural and compressive strength of hardened mortar.

[39] CEN, European Committee for Standardization. EN 12190:1998. Products and systems for the protection and repair of concrete structures. Test methods. Determination of compressive strength of repair mortar.

[40] de Felice G., Aiello M.A., Bellini A., Ceroni F., De Santis S., Garbin E., Leone M., Lignola G.P., Malena M., Mazzotti C., Panizza M., Valluzzi M.R. Experimental characterization of composite-to-brick masonry shear bond. Mater Struct 2016;49(7):2581-2596.

[41] Arboleda D, Carozzi F, Nanni A, Poggi C. Testing Procedures for the Uniaxial Tensile Characterization of Fabric-Reinforced Cementitious Matrix Composites. J Compos Constr 2015;04015063.

[42] Carloni C, Subramaniam KV. Investigation of sub-critical fatigue crack growth in FRP/concrete cohesive interface using digital image analysis. Compos Part B-Eng 2013;51:35-43.

[43] Ghiassi B, Xavier J, Oliveira DV, Lourenço PB. Application of Digital Image Correlation in investigating the bond between FRP and masonry. Compos Struct 2013;106:340-349.

[44] Ghiassi B, Xavier J, Oliveira DV, Kwiecień A, Lourenço PB, Zając B. Evaluation of the bond performance in FRP-brick components re-bonded after initial delamination. Compos Struct 2015;123 271-281.

[45] Napoli A, de Felice G, De Santis S, Realfonzo R. Bond behaviour of Steel Reinforced Polymer strengthening systems. Compos Struct 2016;152:499-515.

[46] Tekieli M, De Santis S, de Felice G, Kwiecień A, Roscini F. Application of Digital Image Correlation to composite reinforcements testing. Compos Struct 2017;160:670-688.

[47] Kwiecień A, de Felice G, Oliveira DV, Zając B, Bellini A, De Santis S, Ghiassi B, Lignola GP, Lourenço PB, Mazzotti C, Prota A. Repair of composite-to-masonry bond using flexible matrix. Mater Struct 2016;49(7):2563-2580.

[48] ICC-ES. AC434 Acceptance criteria for masonry and concrete strengthening using fiber-reinforced cementitious matrix (FRCM) composite systems. ICC-Evaluation Service, Whittier, CA, USA, 2013.

[49] Ascione L, de Felice G, De Santis S. A qualification method for externally bonded Fibre Reinforced Cementitious Matrix (FRCM) strengthening systems. Compos Part B-Eng 2015;78:497-506.

[50] CEN, European Committee for Standardization. EN 1990:2002. Eurocode 0: Basis of structural design.

Figure captions

Figure 1. Textiles (a, b, c) and detail of cord/rope (d, e, f) of steel types G (galvanized steel cords, a,d), S (stainless steel cords, b,e), and R (stainless steel ropes, c,f).

Figure 2. Experimental setups for tensile tests on textile specimens of type G (RM3, a), S (RM3, b) and R (CHI, c, and NAP, d).

Figure 3. Stress-strain response curves of direct tensile tests on dry textile and composite specimens: G textile and GL system (a) and GG system (b), S textile and SP system (c), and R textile and RC system (d).

Figure 4. Experimental setups for direct tensile tests on composite specimens: MIN (a), CER (b), FIR (c), CUT (d), BOL (e), CHI (f), NAP (g), PAD (h), RM3 (i), and SAN (j)

Figure 5. Sketches of failure modes in direct tensile tests on SRG composites.

Figure 6. Crack pattern (a,b,c,d) and failure modes (e,f,g,h) of direct tensile tests. Tests shown in (a,e) were carried out at RM3 on SP system, tests shown in (b,f) were carried out at CHI on RC system, tests shown in (c,g) were carried out at FIR on GG system, and tests in (d,h) were carried out at CUT on GG system.

Figure 7. Experimental setups for shear bond tests on textile specimens: CER (a), CHI (b), CUT (c), RM3 (d), BOL (e), FIR (f), MIN (g), NAP (h), PAD (i), and SAN (j).

Figure 8. Sketches of the failure modes in shear bond tests.

Figure 9. Stress-slip response curves of bond tests on GL (a), GG (b), SP (c), and RC (d) systems.

Figure 10. Failure modes of shear bond tests: cohesive failure of the substrate (a), debonding at the matrix-to-substrate (b) and at the textile-to-matrix (c) interface, textile slippage within the mortar matrix without (d) or with (e) cracking of the outer layer of mortar, tensile rupture of the textile out of the bonded area (f). Tests shown in (a,d,f) were carried out at RM3 on GG (a), SP (d) and GL (f) systems, test shown in (b) was carried out at PAD on GL system, test shown in (c) was carried out at CUT on GG system, and test shown in (e) was carried out at FIR on GG system.

Figure 11. Envelope and average response curves, and identification of qualification point and of secant stiffness for GL (a), GG (b), SP (c), and RC (d) systems.

Figure 12. Mean peak and qualification values for SRG systems: average tensile strength of dry textile and SRG composites, average and characteristic bond strength (qualification stress) (a), strain at peak stress for dry textiles, SRG composites and qualification strain (b), and exploitation of the tensile strength of the composite (c).

Table captions

Table 1. Properties of steel textiles.

Table 2. Mechanical properties of mortar matrices. CV in round brackets.

Table 3. Overview of Round Robin Test programme.

Table 4. Results of tensile tests on textile specimens. CV in round brackets. 5 tests were carried out for each series.

Table 5. Results of direct tensile tests on GL system (galvanized steel cords and lime mortar).

Table 6. Results of direct tensile tests on GG system (galvanized steel cords and geopolymer mortar).

Table 7. Results of direct tensile tests on SP system (stainless steel cords and lime and pozzolan mortar).

Table 8. Results of direct tensile tests on RC system (stainless steel ropes and cement mortar).

Table 9. Results of shear bond tests on GL (galvanized steel cord textile and lime based mortar) system.

Table 10. Results of shear bond tests on GG (galvanized steel cord textile and geopolymer mortar) system.

Table 11. Results of shear bond tests on SP (stainless steel cord textile and pozzolan lime mortar) system.

Table 12. Results of shear bond tests on RC (stainless steel rope textile and cement mortar) system.

Table 13. Qualification parameters.

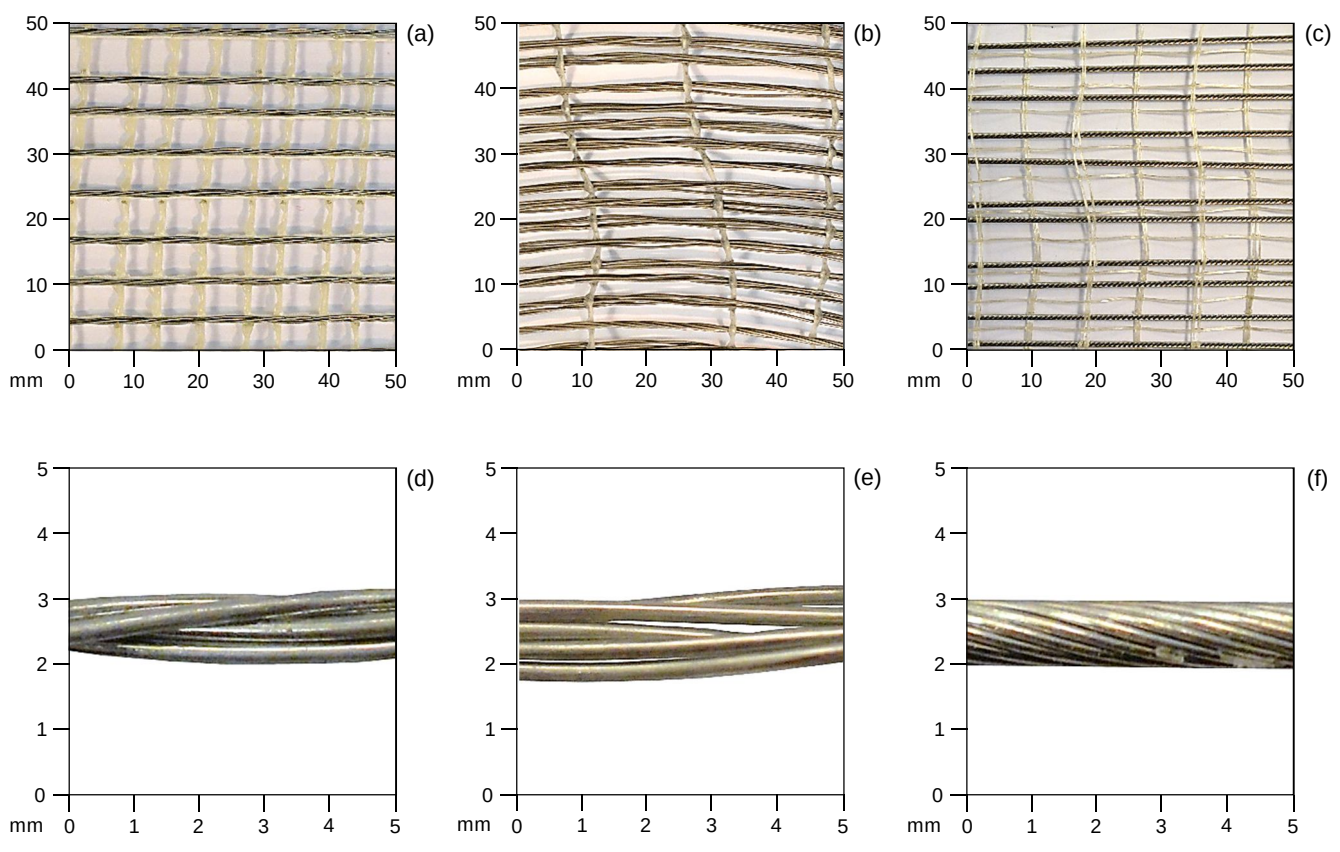
(a)
(b)
(c)
(d)
(e)
(f)
mm
0
10
20
30
40
50
1
2
3
4
5

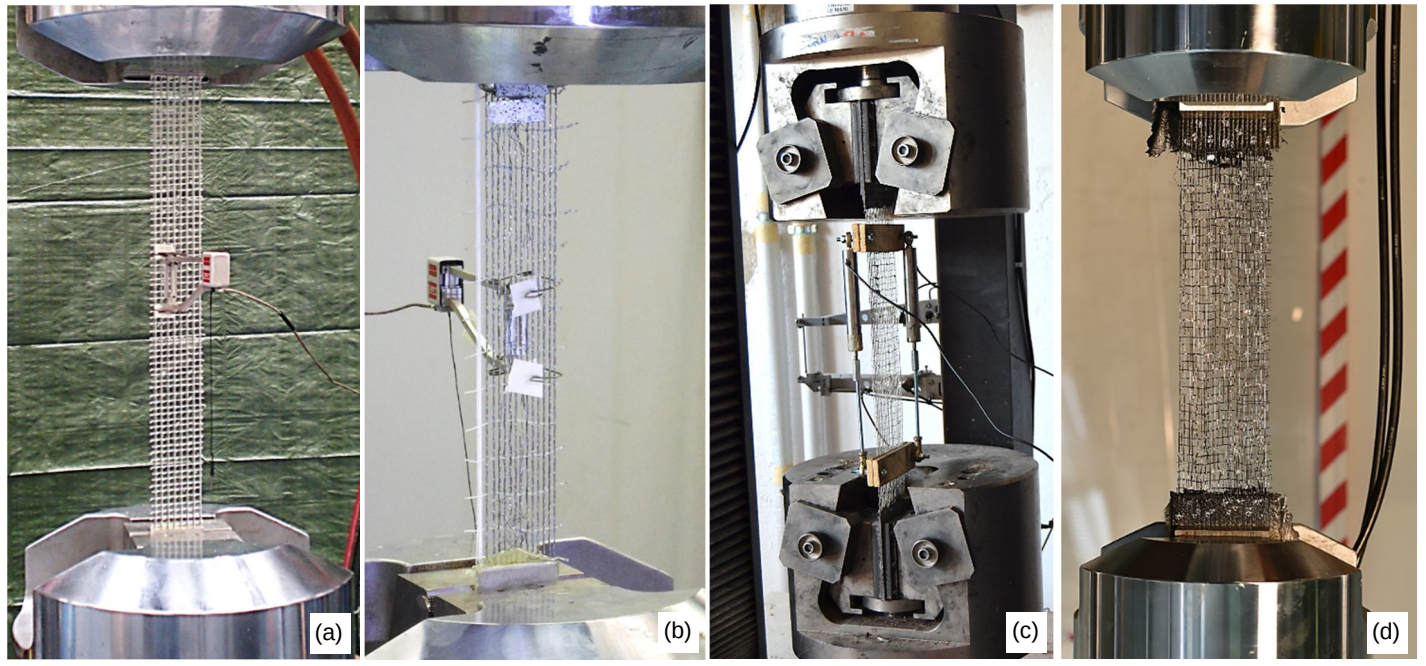
(a)
(b)
(c)
(d)

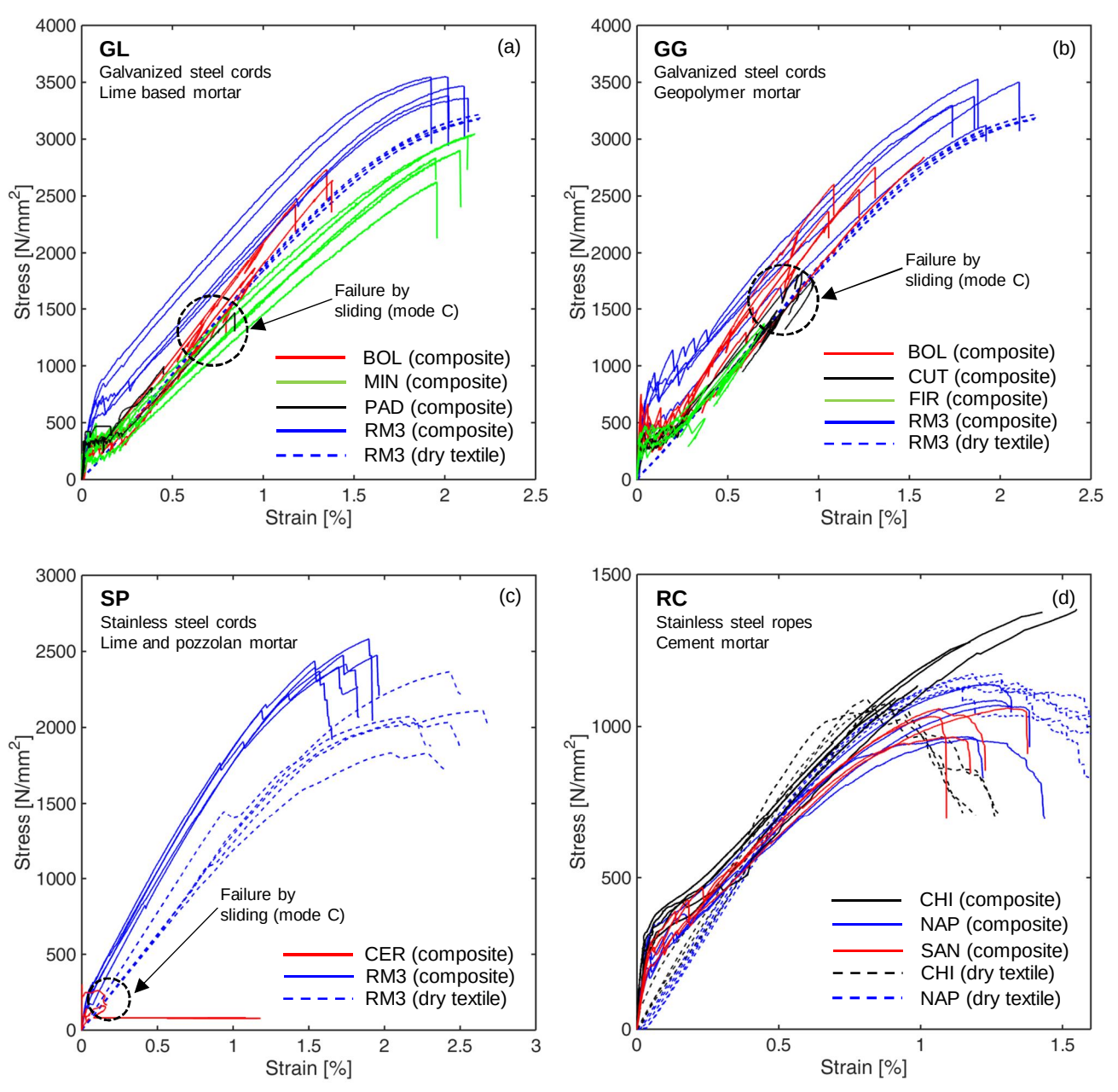
GL
Galvanized steel cords
Lime based mortar
(a)
Failure by
sliding (mode C)
BOL (composite)
MIN (composite)
PAD (composite)
RM3 (composite)
RM3 (dry textile)
Stress [N/mm2]
Strain [%]
GG
Galvanized steel cords
Geopolymer mortar
(b)
Failure by
sliding (mode C)
BOL (composite)
CUT (composite)
FIR (composite)
RM3 (composite)
RM3 (dry textile)
Stress [N/mm2]
Strain [%]
SP
Stainless steel cords
Lime and pozzolan mortar
(c)
Failure by
sliding (mode C)
CER (composite)
RM3 (composite)
RM3 (dry textile)
Stress [N/mm2]
Strain [%]
RC
Stainless steel ropes
Cement mortar
(d)
CHI (composite)
NAP (composite)
SAN (composite)
CHI (dry textile)
NAP (dry textile)
Stress [N/mm2]
Strain [%]


(a)

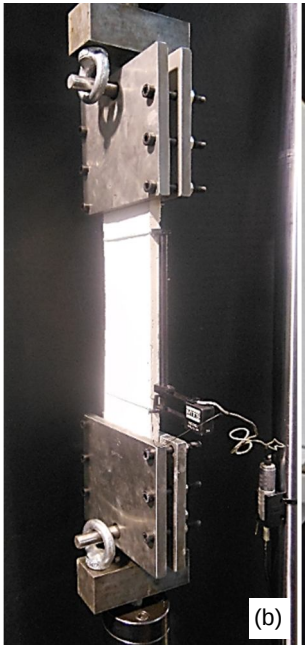
(b)

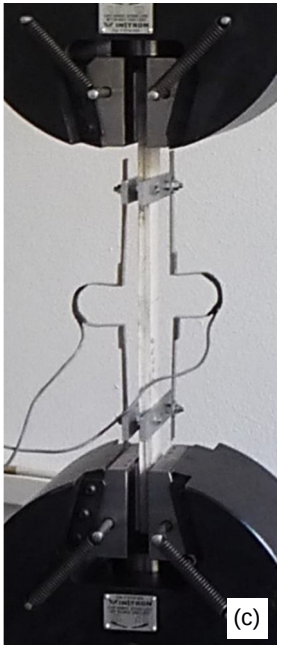
(c)

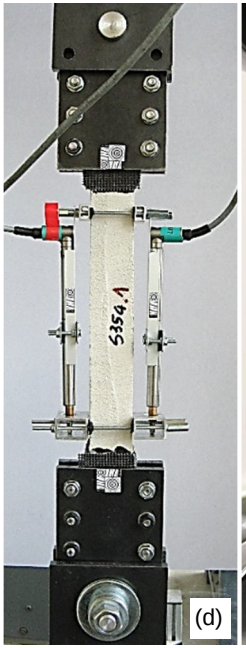

(d)


(e)

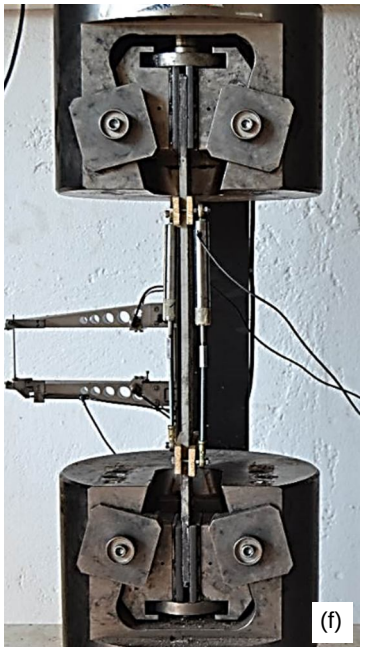
(f)


(g)


(h)

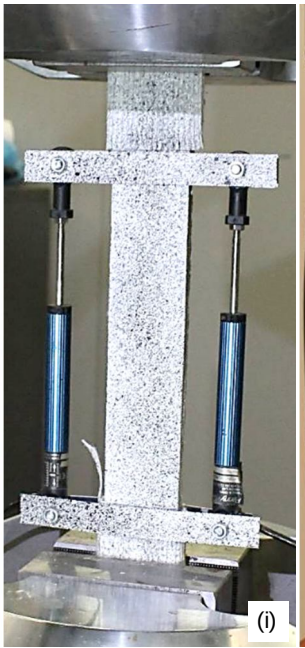
(i)


(j)

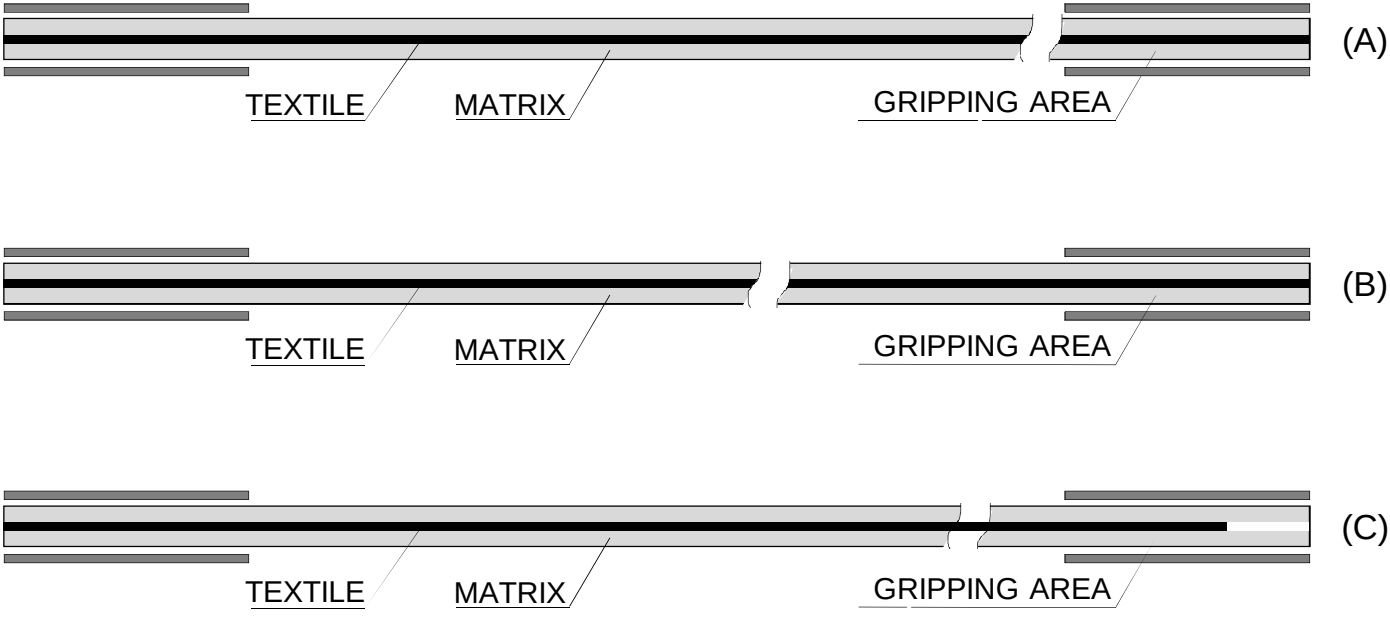
(A)
TEXTILE
MATRIX
GRIPPING AREA
(B)
TEXTILE
MATRIX
GRIPPING AREA
(C)
TEXTILE
MATRIX
GRIPPING AREA

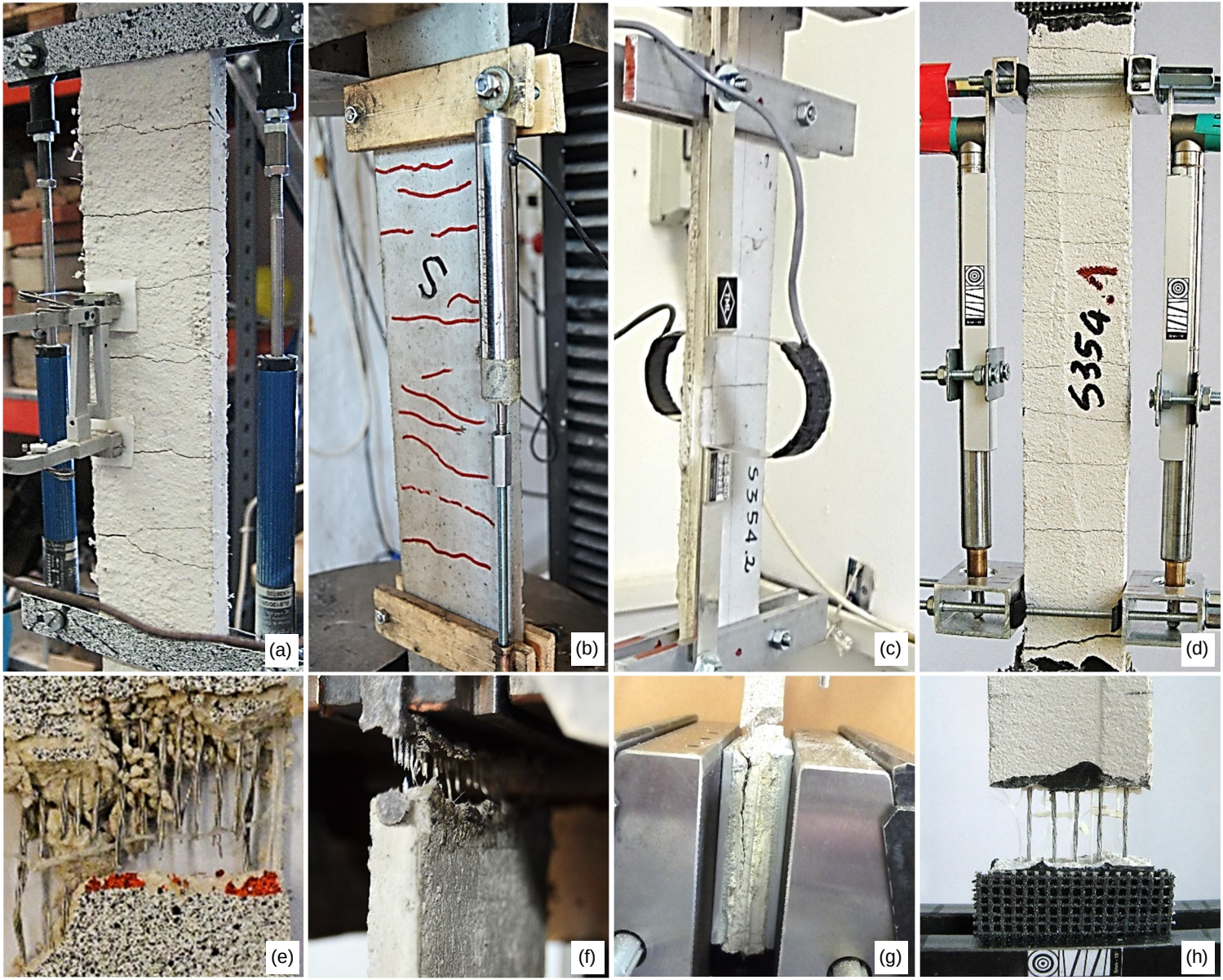
(a)
(b)
S354.2
(c)
S354.1
(d)
(e)
(f)
(g)
(h)

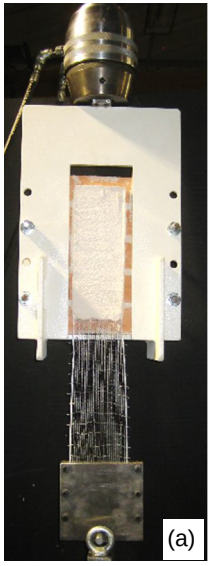
(a)


(b)

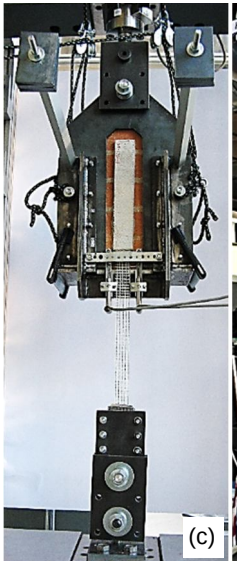
(c)

(d)

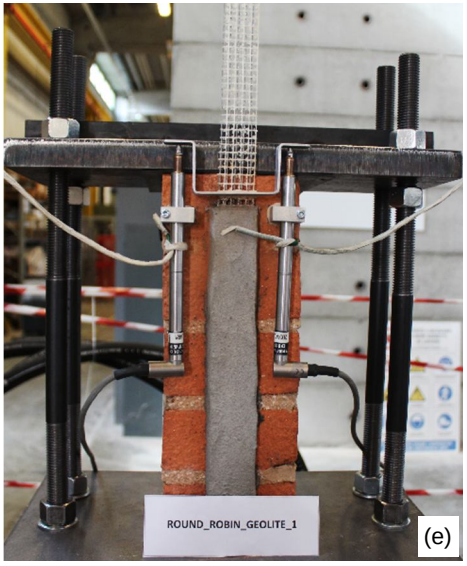

(e)

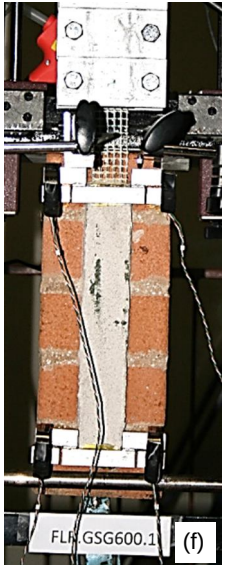

(f)

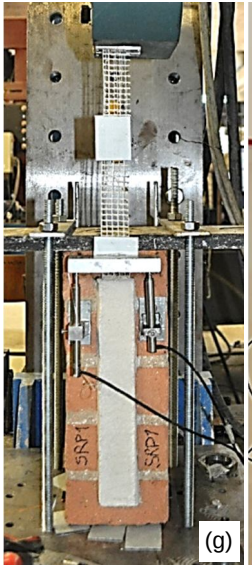

(g)

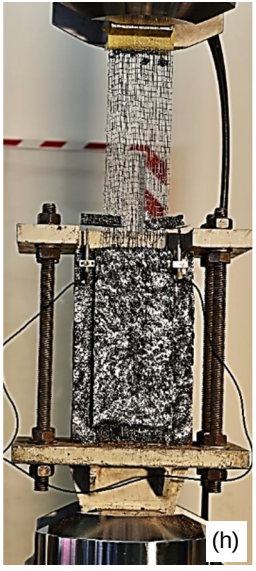
(h)

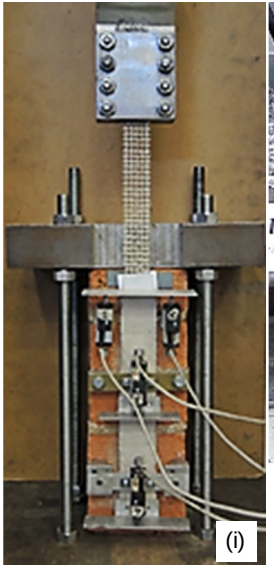
(i)

(j)

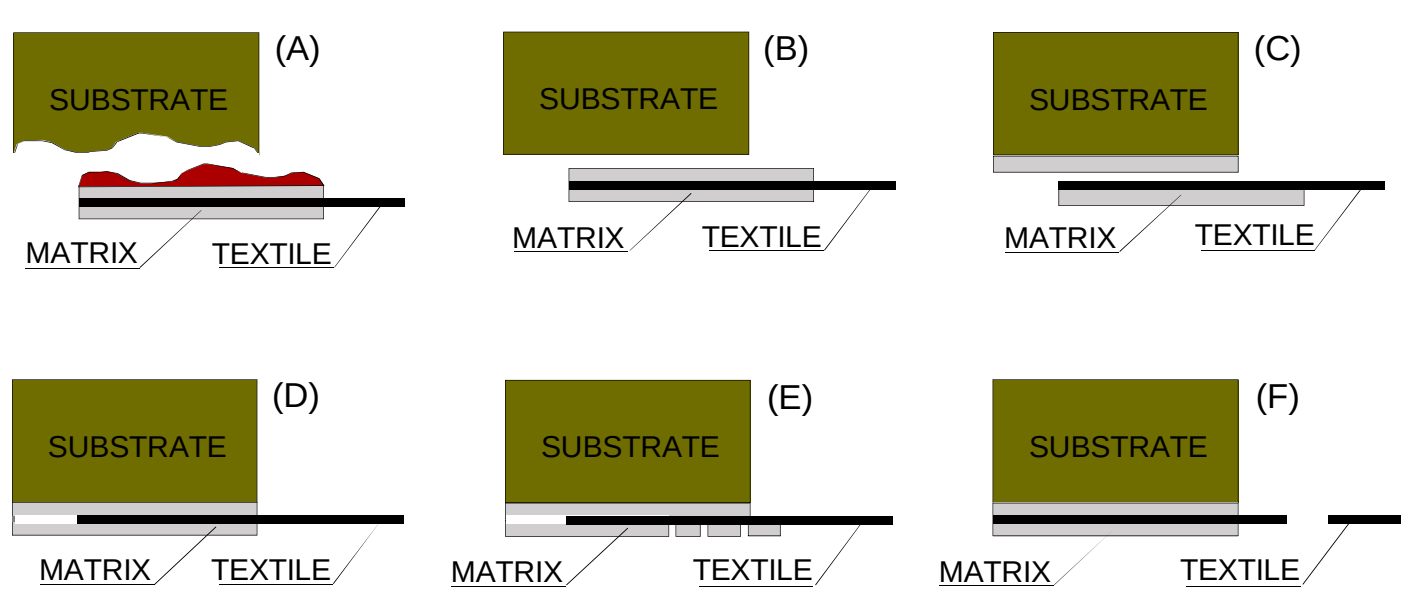
(A)
SUBSTRATE
MATRIX
TEXTILE
(B)
SUBSTRATE
MATRIX
TEXTILE
(C)
SUBSTRATE
MATRIX
TEXTILE
(D)
SUBSTRATE
MATRIX
TEXTILE
(E)
SUBSTRATE
MATRIX
TEXTILE
(F)
SUBSTRATE
MATRIX
TEXTILE

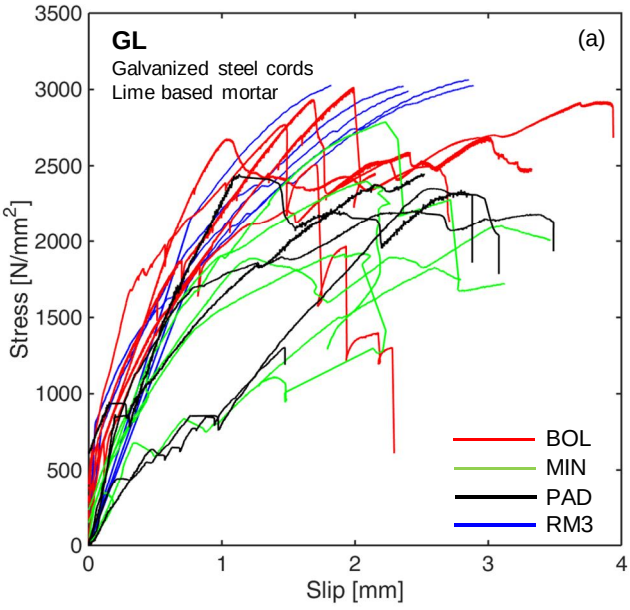
GL
Galvanized steel cords
Lime based mortar
(a)
Stress [N/mm^2]
Slip [mm]
BOL
MIN
PAD
RM3

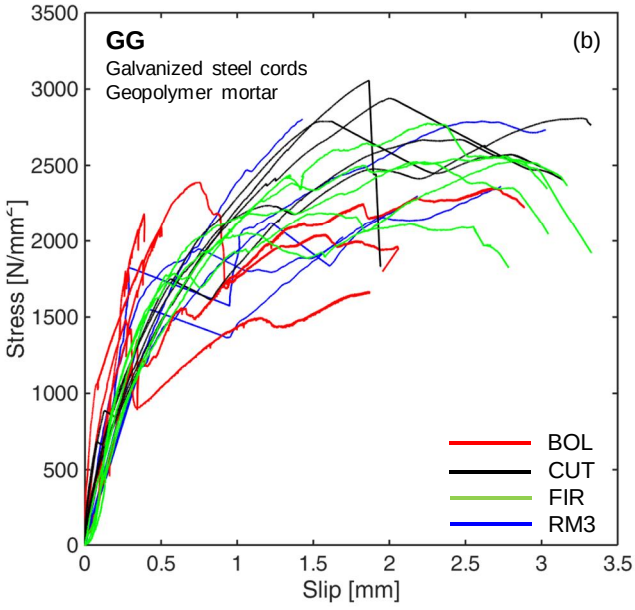
GG
Galvanized steel cords
Geopolymer mortar
(b)
Stress [N/mm^2]
Slip [mm]
BOL
CUT
FIR
RM3

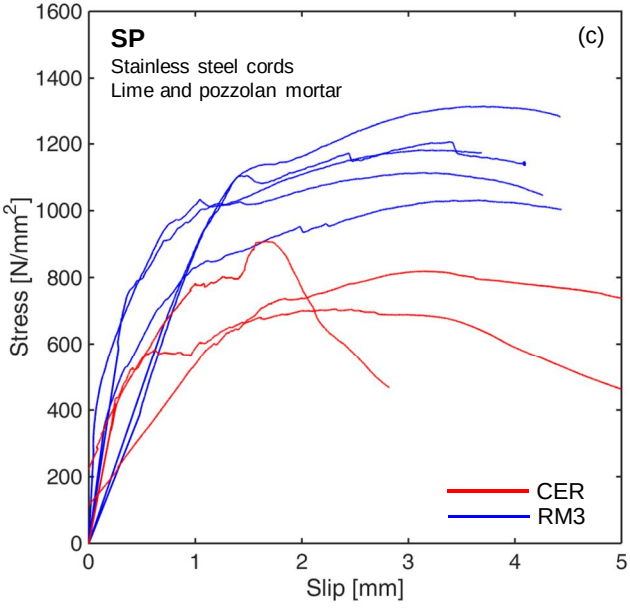
SP
Stainless steel cords
Lime and pozzolan mortar
(c)
Stress [N/mm^2]
Slip [mm]
CER
RM3

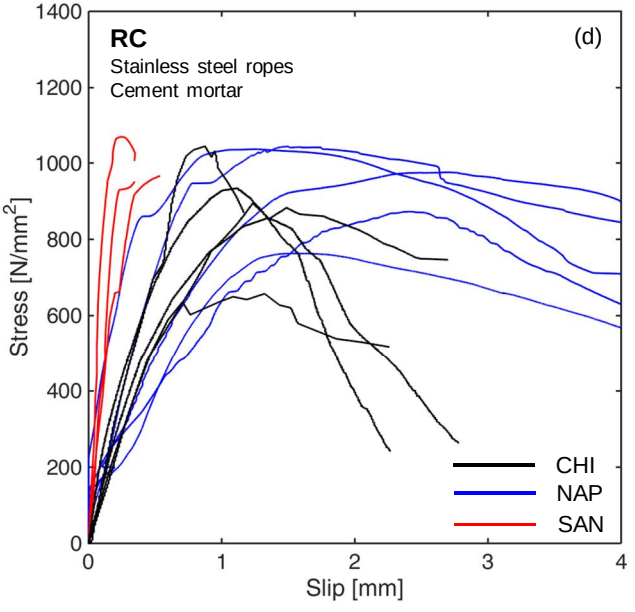
RC
Stainless steel ropes
Cement mortar
(d)
Stress [N/mm^2]
Slip [mm]
CHI
NAP
SAN


(a)


(b)

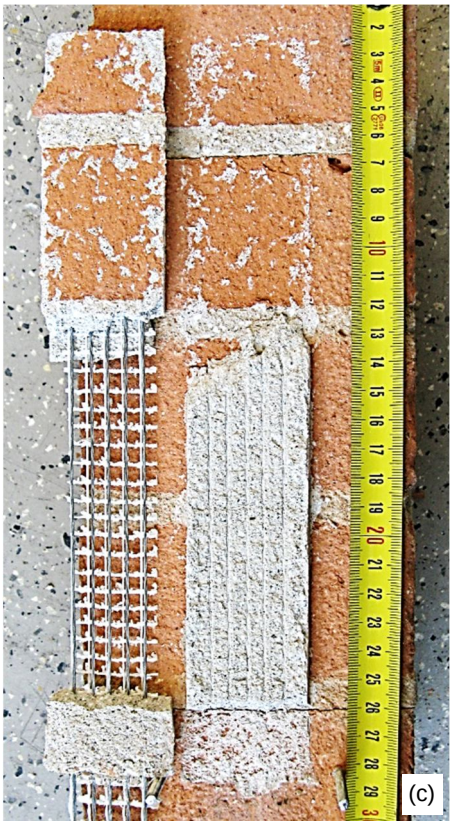
(c)


(d)


(e)


(f)

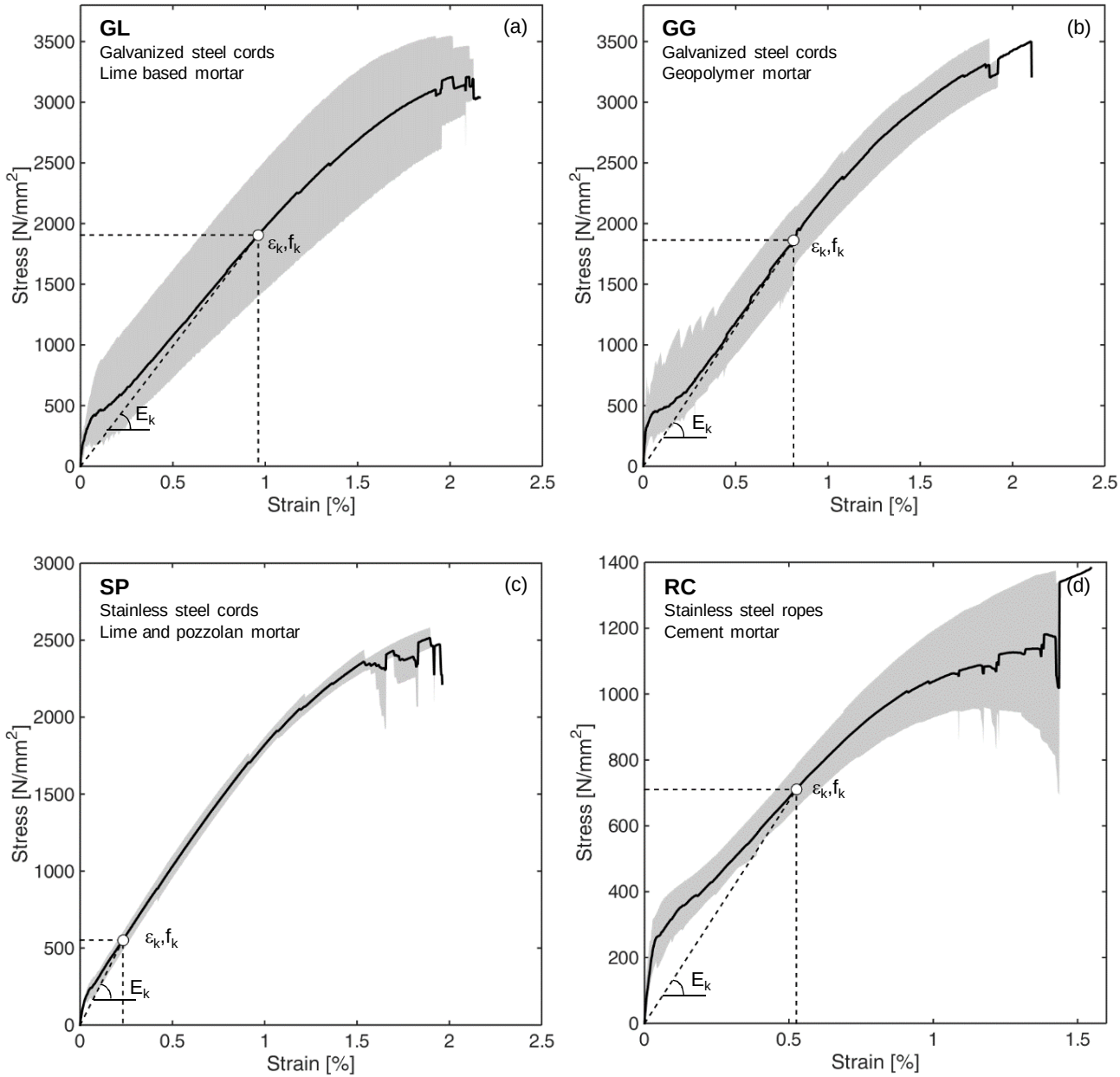
GL
Galvanized steel cords
Lime based mortar
(a)
Stress [N/mm2]
Strain [%]
εk,fk
Ek
GG
Galvanized steel cords
Geopolymer mortar
(b)
SP
Stainless steel cords
Lime and pozzolan mortar
(c)
RC
Stainless steel ropes
Cement mortar
(d)

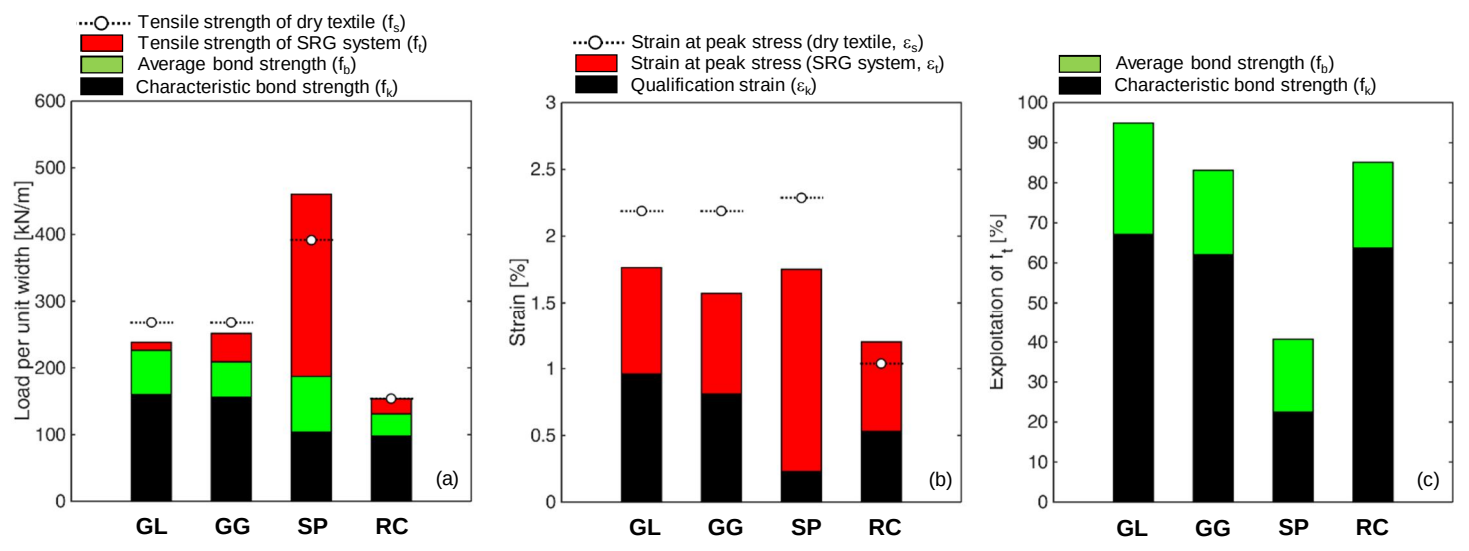
Tensile strength of dry textile (f_s)
Tensile strength of SRG system (f_t)
Average bond strength (f_b)
Characteristic bond strength (f_k)
Load per unit width [kN/m]
600
500
400
300
200
100
0
GL
GG
SP
RC
(a)
Strain at peak stress (dry textile, ε_s)
Strain at peak stress (SRG system, ε_t)
Qualification strain (ε_k)
Strain [%]
3
2.5
2
1.5
1
0.5
0
GL
GG
SP
RC
(b)
Average bond strength (f_b)
Characteristic bond strength (f_k)
Exploitation of f_t [%]
100
90
80
70
60
50
40
30
20
10
0
GL
GG
SP
RC
(c)

Table 1. Properties of steel textiles.

Textile	Label	c [cords/mm]	i [mm]	γ [kg/m^2]	t [mm]
Galvanized carbon steel cords	G	0.157	6.35	670	0.084
Stainless steel cords	S	0.315	3.18	1500	0.188
Stainless steel ropes	R	0.200	5.00	1057	0.138

Table 2. Mechanical properties of mortar matrices. CV in round brackets.

Mortar	Label	f_{cm} [N/mm^2]	E_{cm} [kN/mm^2]	f_{tm} [N/mm^2]
Lime based mortar with geopolymeric binders	L	20.6 (4%)	11.42 (5%)	5.42 (4%)
Geopolymer mortar	G	56.3 (3%)	22.01 (8%)	10.31 (3%)
Lime and pozzolan based mortar	P	6.4 (10%)	6.31 (8%)	1.24 (12%)
Fibre-reinforced cement mortar with polymeric additives	C	22.7 (7%)	10.0[a]	11.2 (6%)

[a] From Technical Data Sheet

Table 3. Overview of Round Robin Test programme.

Institution			Tested systems			
Name	Acronym	Country	GL	GG	SP	RC
University of Bologna	BOL	Italy	$5T^{S}+5B^{S}$	$5T^{S}+5B^{S}$		
CertiMaC	CER	Italy			$5T^{L}+5B^{L}$	
University of Chieti-Pescara	CHI	Italy				5F+ $5T^{L}+5B^{L}$
Cracow University of Technology	CUT	Poland		$5T^{S}+5B^{S}$		
University of Firenze	FIR	Italy		$5T^{S}+5B^{S}$		
University of Minho	MIN	Portugal	5T+5B			
University of Naples	NAP	Italy				5F+ $5T^{L}+5B^{L}$
University of Padova	PAD	Italy	$5T^{S}+5B^{S}$			
Roma Tre University	RM3	Italy	5M+5F+ $5T^{S}+5B^{S}$	5M+5F+ $5T^{S}+5B^{S}$	5M+5F+ $5T^{L}+5B^{L}$	
University of Sannio	SAN	Italy				$5T^{L}+5B^{L}$
Total			5M+5F+ 20T+20B	5M+5F+ 20T+20B	5M+5F+ 20T+20B	5F+ 20T+20B

Table 4. Results of tensile tests on textile specimens. CV in round brackets. 5 tests were carried out for each series.

Textile	Institution	f_s [N/mm^2]	F_s [kN/m]	E_s [kN/mm^2]	ε_s [%]
Galvanized steel cords (G)	RM3	3191 (1%)	268	186 (1%)	2.19 (1%)
Stainless steel cords (S)	RM3	2084 (9%)	392	130 (11%)	2.29 (11%)
Stainless steel ropes (R)	CHI	1069 (2%)	148	144 (6%)	0.86 (5%)
	NAP	1150 (2%)	159	147 (2%)	1.18 (6%)

Table 5. Results of direct tensile tests on GL system (galvanized steel cords and lime mortar).

Specimen	Stage I			Stage II			Stage III					FM
	σ_I [N/mm^2]	ε_I [%]	E_I [kN/mm^2]	σ_{II} [N/mm^2]	ε_{II} [%]	E_{II} [kN/mm^2]	f_t [N/mm^2]	F_t [kN/m]	ε_t [%]	E_{III} [kN/mm^2]	d [mm]	
GL-BOL-1	299	0.020	1495	248	0.081	-	2421	203	1.17	199	29	A-C
GL-BOL-2	199	0.012	1692	376	0.198	95	-	-	-	-	55	C
GL-BOL-3	294	0.014	2082	288	0.219	-	-	-	-	-	22	C
GL-BOL-4	212	0.026	911	214	0.175	-	2620	220	1.38	200	25	C
GL-BOL-5	394	0.017	2355	378	0.164	-	2733	230	1.35	199	23	A-C
Average	280	0.018	1708	301	0.167	95	2592	218	1.30	199	31	
CV	28%	31%	33%	25%	32%	-	8%	8%	10%	1%	45%	
GL-MIN-1	197	0.053	371	297	0.220	60	2623	220	1.96	180	21	B
GL-MIN-2	497	0.079	632	494	0.330	99	2836	238	1.95	165	22	B
GL-MIN-3	-	-	-	465	0.200	132	3024	254	2.10	155	20	B
GL-MIN-4	408	0.065	627	483	0.310	54	2900	243	2.08	186	21	B
GL-MIN-5	416	0.036	1156	450	0.220	49	3049	256	2.16	152	19	B
Average	380	0.058	697	438	0.256	169	2887	243	2.05	4046	21	
CV	34%	31%	47%	18%	23%	111%	6%	6%	4%	195%	6%	
GL-PAD-1	330	0.014	2433	394	0.228	29	1467	123	0.757	174	23	C
GL-PAD-2	328	0.014	2279	344	0.128	14	1027	86	0.453	199	39	C
GL-PAD-3	422	0.021	2043	511	0.203	61	807	67	0.388	157	25	C
Average	360	0.016	2252	416	0.186	78	1101	92	0.53	777	29	
CV	15%	25%	9%	21%	28%	76%	31%	31%	37%	136%	30%	
GL-RM3-1	882	0.111	795	1062	0.209	178	3545	297	1.92	192	18	A
GL-RM3-2	699	0.077	1026	763	0.205	71	3466	291	2.10	192	17	A
GL-RM3-3	738	0.115	667	873	0.295	93	3383	284	2.02	184	40	A-B
GL-RM3-4	467	0.042	1220	659	0.181	137	3360	282	2.13	169	-	A-B
GL-RM3-5	574	0.054	860	1004	0.234	171	3551	298	2.00	185	33	A-B
Average	672	0.080	914	872	0.225	130	3461	290	2.03	184	27	
CV	24%	41%	23%	19%	19%	36%	3%	3%	4%	5%	42%	
Total average	408	0.043	1258	489	0.200	83	2838	238	1.76	172	25	
Total CV	48%	79%	54%	52%	30%	61%	13%	13%	18%	9%	40%	
Mean CV	25%	32%	28%	21%	25%	50%	5%	5%	6%	6%	31%	

Table 6. Results of direct tensile tests on GG system (galvanized steel cords and geopolymer mortar).

Specimen	Stage I			Stage II			Stage III					FM
	σ_I [N/mm^2]	ε_I [%]	E_I [kN/mm^2]	σ_{II} [N/mm^2]	ε_{II} [%]	E_{II} [kN/mm^2]	f_t [N/mm^2]	F_t [kN/m]	ε_t [%]	E_{III} [kN/mm^2]	d [mm]	
GG-BOL-1	522	0.017	3122	489	0.286	-	2182	183	1.09	162	26	A
GG-BOL-2	506	0.017	2979	511	0.238	-	2744	230	1.31	173	27	A
GG-BOL-3	723	0.022	3287	469	0.187	-	2576	216	1.07	201	36	A
GG-BOL-4	520	0.023	2262	446	0.212	-	2813	236	1.57	174	34	A
GG-BOL-5	661	0.026	2544	575	0.202	-	2364	199	1.05	178	35	A
Average	587	0.021	2839	2380	0.225	-	2536	573	1.22	178	32	
CV	17%	19%	15%	110%	17%	-	10%	139%	18%	8%	15%	
GG-CUT-1	414	0.038	1105	476	0.230	32	1836	154	0.91	199	19	C
GG-CUT-2	247	0.012	2083	480	0.220	112	1488	125	0.77	183	19	C
GG-CUT-3	336	0.061	554	475	0.250	73	1754	147	0.97	178	21	C
GG-CUT-4	368	0.013	2871	511	0.270	56	1390	117	0.75	185	20	C
GG-CUT-5	281	0.014	1997	490	0.250	88	1463	123	0.79	179	18	C
Average	329	0.028	1722	486	0.244	72	1586	133	0.84	185	19	
CV	20%	78%	52%	3%	8%	42%	12%	12%	12%	5%	6%	
GG-FIR-1	410	0.025	1738	525	0.285	49	954	80	0.52	179	25	C-A
GG-FIR-2	416	0.018	2381	477	0.195	65	825	69	0.39	178	30	C-A
GG-FIR-3	254	0.017	1463	367	0.200	109	538	45	0.37	149	27	C-A
GG-FIR-4	249	0.016	1611	407	0.210	68	1373	115	0.70	200	21	C-A
GG-FIR-5	397	0.017	2250	451	0.249	75	1155	97	0.62	188	21	C-A
Average	345	0.019	1889	445	0.227	73	969	81	0.5198	179	25	
CV	25%	20%	21%	13%	17%	30%	33%	33%	28%	10%	16%	
GG-RM3-1	701	0.046	1561	1326	0.418	168.1	3528	296	1.88	194	33	A
GG-RM3-2	498	0.069	1943	680	0.243	93.0	3122	262	1.92	195	33	A-B
GG-RM3-3	752	0.105	1670	754	0.144	129.4	3375	283	1.86	179	27	A-B
GG-RM3-4	862	0.114	1290	1036	0.285	107.9	3298	277	1.74	186	50	A-B
GG-RM3-5	869	0.068	2125	1039	0.312	97.5	3501	294	2.10	175	25	A
Average	736	0.080	1718	967	0.280	119	3365	282	1.90	186	34	
CV	20%	35%	19%	27%	35%	26%	5%	5%	7%	5%	29%	
Total average	499	0.037	2042	599	0.244	88	2950.5	248	1.56	182	27.3	
Total CV	40%	83%	34%	42%	23%	39%	16%	16%	25%	7%	29%	
Mean CV	20%	38%	27%	13%	19%	33%	7%	7%	12%	7%	16%	

Table 7. Results of direct tensile tests on SP system (stainless steel cords and lime and pozzolan mortar).

Specimen	Stage I			Stage II			Stage III					FM
	σ_I [N/mm^2]	ε_I [%]	E_I [kN/mm^2]	σ_{II} [N/mm^2]	ε_{II} [%]	E_{II} [kN/mm^2]	f_t [N/mm^2]	F_t [kN/m]	ε_t [%]	E_{III} [kN/mm^2]	d [mm]	
SP-CER-1	299	0.059	799	-	-	-	301	56	1.44	-	34	C
SP-CER-2	142	0.088	200	-	-	-	242	45	6.01	-	29	C
SP-CER-3	144	0.013	265	-	-	-	145	27	0.14	-	31	C
SP-CER-4	160	0.036	117	-	-	-	162	30	0.35	-	36	C
SP-CER-5	94	0.014	177	-	-	-	94	17	0.35	-	29	C
Average	168	0.042	312	-	-	-	189	35	1.66	-	32	
CV	46%	76%	89%	-	-	-	43%	43%	150%	-	10%	
SP-RM3-1	272	0.051	556	277	0.086	16	2475	465	1.70	174	31	A-B
SP-RM3-2	188	0.027	692	-	-	-	2416	454	1.87	181	30	A-B
SP-RM3-3	140	0.028	505	-	-	-	2370	445	1.63	184	31	A
SP-RM3-4	184	0.028	492	-	-	-	2582	485	1.85	171	25	A
SP-RM3-5	158	0.035	492	176	0.077	29	2398	451	1.71	178	37	A
Average	188	0.034	547	226	0.081	22	2448	460	1.75	178	31	
CV	27%	30%	15%	31%	8%	43%	3%	3%	6%	3%	14%	
Total average	178	0.038	429	226	0.081	22	2448	460	1.75	178	31	
Total CV	35%	60%	53%	31%	8%	43%	3%	3%	6%	3%	11%	
Mean CV	36%	53%	52%	31%	8%	43%	3%	3%	6%	3%	12%	

Table 8. Results of direct tensile tests on RC system (stainless steel ropes and cement mortar).

Specimen	Stage I			Stage II			Stage III					FM
	σ_I [N/mm^2]	ε_I [%]	E_I [kN/mm^2]	σ_{II} [N/mm^2]	ε_{II} [%]	E_{II} [kN/mm^2]	f_t [N/mm^2]	F_t [kN/m]	ε_t [%]	E_{III} [kN/mm^2]	d [mm]	
RC-CHI-1	311	0.039	798	480	0.224	91	1375	189	1.427	92	34	A
RC-CHI-2	274	0.030	913	530	0.404	69	1384	191	1.549	92	-	A
RC-CHI-3	303	0.028	1084	472	0.197	100	1278	176	1.172	94	30	A
RC-CHI-4	325	0.042	775	420	0.156	83	1092	151	0.912	94	29	A
RC-CHI-5	280	0.035	800	368	0.171	65	1133	156	0.990	97	31	A
Average	299	0.035	874	454	0.230	82	1252	173	1.210	94	31	
CV	7%	17%	15%	13%	43%	18%	11%	11%	23%	2%	7%	
RC-NAP-1	204	0.049	736	300	0.150	93	1139	157	1.240	115	130	B
RC-NAP-2	346	0.062	1015	425	0.200	55	967	133	1.170	91	-	A
RC-NAP-3	306	0.041	1028	540	0.380	71	1087	150	1.270	104	100	B
RC-NAP-4	202	0.035	777	300	0.140	95	961	133	1.180	97	100	B
RC-NAP-5	240	0.045	904	400	0.260	73	1070	148	1.280	103	100	B
Average	260	0.046	892	393	0.226	77	1045	144	1.228	102	108	
CV	24%	22%	15%	25%	43%	21%	7%	7%	4%	9%	14%	
RC-SAN-1	288	0.050	576	515	0.313	86	1033	143	1.04	85	-	A
RC-SAN-2	201	0.049	480	731	0.567	101	965	133	1.11	71	-	A
RC-SAN-3	277	0.049	589	606	0.462	79	1067	147	1.3	83	-	A
RC-SAN-4	263	0.046	496	545	0.344	97	1058	146	1.07	83	-	A
Average	257	0.049	535	599	0.422	91	1031	142	1.130	81	-	
CV	15%	3%	10%	16%	27%	11%	4%	4%	10%	8%	-	
Total average	273	0.04	783	473	0.28	83	1115	154	1.19	93	69	
Total CV	17%	21%	25%	25%	46%	17%	12%	12%	14%	11%	61%	
Mean CV	15%	14%	13%	18%	38%	17%	7%	7%	12%	6%	10%	

Table 9. Results of shear bond tests on GL (galvanized steel cord textile and lime based mortar) system.

Specimen	f_b [N/mm^2]	F_b [kN/m]	s [mm]	$\eta_s=f_b/f_s$ [%]	$\eta_t=f_b/f_t$ [%]	FM
GL-B-BOL-1	2772	233	1.47	87	98	F
GL-B-BOL-2	2936	247	1.69	92	103	C
GL-B-BOL-3	3015	253	1.99	94	106	F
GL-B-BOL-4	2921	245	3.84	91	103	C
GL-B-BOL-5	2678	225	1.04	84	94	C
Average	2865	240	2.01	91	102	
CV	3%	3%	48%	3%	3%	
GL-B-MIN-1	1921	161	2.03	60	68	D
GL-B-MIN-2	2398	201	2.06	75	84	F
GL-B-MIN-3	2788	234	2.22	87	98	F
GL-B-MIN-4	2100	176	3.09	66	74	E
GL-B-MIN-5	1825	153	2.59	57	64	E
Average	2206	185	2.40	72	81	
CV	17%	17%	21%	16%	16%	
GL-B-PAD-1	2450	206	2.50	77	86	B
GL-B-PAD-2	2208	185	1.27	69	78	C
GL-B-PAD-3	2445	205	1.13	76	86	B-C
GL-B-PAD-4	2352	197	2.57	74	83	B-C
Average	2364	198	1.87	74	83	
CV	5%	5%	41%	5%	5%	
GL-B-RM3-1	3062	257	2.85	96	108	F
GL-B-RM3-2	3022	253	2.36	95	106	F
GL-B-RM3-3	3026	254	2.89	95	106	F
GL-B-RM3-4	2989	251	2.40	94	105	F-C
GL-B-RM3-5	3025	254	1.82	95	106	F
Average	3025	254	2.46	95	107	
CV	1%	1%	18%	1%	1%	
Total average	2628	220	2.04	84	94	
Total CV	15%	15%	35%	15%	15%	
Mean CV	7%	7%	28%	7%	7%	

Table 10. Results of shear bond tests on GG (galvanized steel cord textile and geopolymer mortar) system.

Specimen	f_b [N/mm^2]	F_b [kN/m]	s [mm]	$\eta_s=f_b/f_s$ [%]	$\eta_t=f_b/f_t$ [%]	FM
GG-B-BOL-1	1670	140	1.86	52	56	B-A
GG-B-BOL-2	2184	183	0.39	68	73	B-A
GG-B-BOL-3	2391	201	0.75	75	80	C
GG-B-BOL-4	2356	198	2.69	74	78	B-C
GG-B-BOL-5	2094	176	0.50	65	70	B-A
Average	2139	180	1.24	67	71	
CV	13%	13%	81%	13%	13%	
GG-B-CUT-1	2809	236	3.25	88	94	C-A
GG-B-CUT-2	2669	224	2.46	83	89	C-B
GG-B-CUT-3	2939	247	2.00	92	98	C-E
GG-B-CUT-4	2789	234	1.55	87	93	C-E
GG-B-CUT-5	3056	257	1.87	96	102	F
Average	2852	239	2.23	89	95	
CV	5%	5%	29%	5%	5%	
GG-B-FIR-1	2114	177	2.13	66	71	E-C
GG-B-FIR-2	2777	233	2.24	87	93	E-C
GG-B-FIR-3	2525	212	2.24	79	84	E-C
GG-B-FIR-4	2563	215	2.74	80	85	E-C
GG-B-FIR-5	2536	213	2.85	79	85	E-C
Average	2503	210	2.44	78	84	
CV	9%	9%	13%	9%	9%	
GG-B-RM3-1	2025	170	1.69	63	67	B-A
GG-B-RM3-2	2299	193	2.19	72	77	B-A
GG-B-RM3-3	2362	198	2.73	74	79	A-C
GG-B-RM3-4	2808	236	1.43	88	94	F
GG-B-RM3-5	2789	234	2.61	87	93	B-A
Average	2457	206	2.13	77	82	
CV	13%	13%	26%	13%	13%	
Total average	2488	209	2.01	78	83	
Total CV	14%	14%	39%	14%	14%	
Mean CV	10%	10%	37%	10%	10%	

Table 11. Results of shear bond tests on SP (stainless steel cord textile and pozzolan lime mortar) system.

Specimen	f_b [N/mm^2]	F_b [kN/m]	s [mm]	$\eta_s=f_b/f_s$ [%]	$\eta_t=f_b/f_t$ [%]	FM
SP-B-CER-1	819	154	3.15	39	33	E
SP-B-CER-2	689	129	-	33	28	E
SP-B-CER-3	705	133	2.32	34	29	E
SP-B-CER-4	908	171	1.66	44	37	E
Average	780	146	2.41	38	32	
CV	13%	13%	31%	13%	13%	
SP-B-RM3-1	1113	209	3.15	53	45	D
SP-B-RM3-2	1312	247	3.70	63	54	D
SP-B-RM3-3	1206	227	3.38	58	49	D
SP-B-RM3-4	1032	194	3.66	49	42	D
SP-B-RM3-5	1182	222	3.11	57	48	D
Average	1169	220	3.40	56	48	
CV	9%	9%	8%	9%	9%	
Total average	996	187	3.02	48	41	
Total CV	23%	23%	23%	23%	23%	
Mean CV	11%	11%	20%	11%	11%	

Table 12. Results of shear bond tests on RC (stainless steel rope textile and cement mortar) system.

Specimen	f_b [N/mm^2]	F_b [kN/m]	s [mm]	$\eta_s=f_b/f_s$ [%]	$\eta_t=f_b/f_t$ [%]	FM
RC-B-CHI-1	934	129	1.15	84	84	F
RC-B-CHI-2	856	118	1.37	77	77	F
RC-B-CHI-3	658	91	1.35	59	59	F
RC-B-CHI-4	894	123	1.27	80	80	F
RC-B-CHI-5	1044	144	0.92	94	94	F
Average	877	121	1.21	79	79	
CV	16%	16%	15%	16%	16%	
RC-B-NAP-1	770	106	1.53	69	69	D
RC-B-NAP-2	872	120	2.41	78	78	D
RC-B-NAP-3	1036	143	1.24	93	93	D
RC-B-NAP-4	1044	144	1.50	94	94	D
RC-B-NAP-5	976	135	2.71	88	88	D
Average	939	130	1.88	84	84	
CV	12%	12%	34%	12%	12%	
RC-B-SAN-1	968	134	0.53	87	87	F
RC-B-SAN-2	1068	147	0.24	96	96	F
RC-B-SAN-3	949	131	0.34	85	85	F
RC-B-SAN-4	1087	150	-	97	97	F
RC-B-SAN-5	1084	149	-	97	97	D-E
Average	1031	142	0.37	92	92	
CV	6%	6%	40%	6%	6%	
Total average	949	131	1.15	85	85	
Total CV	13%	13%	62%	13%	13%	
Mean CV	12%	12%	30%	12%	12%	

Table 13. Qualification parameters.

SRG system	Specimens	k_n [-]	f_k [N/mm^2]	F_k [kN/m]	ε_k [%]	E_k [kN/mm^2]
GL	19	1.78	1906	160	0.96	198
GG	20	1.76	1864	157	0.81	229
SP	9	1.96	552	104	0.23	238
RC	15	1.84	710	98	0.53	135